

VILNIUS UNIVERSITY
CENTER FOR PHYSICAL SCIENCES AND TECHNOLOGY

SIMA REKŠTYTĖ

**THE DEVELOPMENT AND APPLICATIONS OF THE
METHODS OF DIRECT LASER WRITING USING
FEMTOSECOND LIGHT PULSES IN TRANSPARENT
CROSS-LINKABLE MATERIALS**

Summary of Doctoral Dissertation
Physical Sciences, Physics (02P)

Vilnius, 2016

The doctoral dissertation was prepared at Vilnius University during 2012–2016.

Scientific supervisor – Prof. Dr. Roaldas Gadonas (Vilnius University, Physical Sciences, Physics – 02P).

Doctoral committee:

Chairman – Prof. Habil. Dr. Valdas Sirutkaitis (Vilnius University, Physical Sciences, Physics – 02P).

Members:

- Dr. Justinas Čeponkus (Vilnius University, Physical Sciences, Physics – 02P);
- Prof. Habil. Dr. Juozas Vidas Gražulevičius (Kaunas University of Technology, Physical Sciences, Chemistry – 03P);
- Prof. Janis Spigulis (University of Latvia, Physical Sciences, Physics – 02P);
- Dr. Roland Tomašiūnas (Vilnius University, Physical Sciences, Physics – 02P).

The dissertation will be defended under open consideration in the Council of Physics on the 27th of September, 2016, 15 p.m. at the Laser Research Center, Vilnius University, room 306.

Address: Saulėtekio Ave. 10, Vilnius, Lithuania.

The summary of the dissertation was distributed on the 26th of August, 2016.

The dissertation is available at the libraries of Vilnius University and Center for Physical Sciences and Technology, and also at Vilnius University website: www.vu.lt/lt/naujienos/ivykiu-kalendorius.

VILNIAUS UNIVERSITETAS
FIZINIŲ IR TECHNOLOGIJOS MOKSLŲ CENTRAS

SIMA REKŠTYTĖ

**TIESIOGINIO LAZERINIO RAŠYMO
FEMTOSEKUNDINIAIS ŠVIESOS IMPULSAIS
SKAIDRIOSE TINKLINAMOSE MEDŽIAGOSE
METODŲ VYSTYMAS IR TAIKYMAI**

Daktaro disertacijos santrauka
Fiziniai mokslai, Fizika (02P)

Vilnius, 2016

Disertacija rengta 2012–2016 metais Vilniaus universitete.

Mokslinis vadovas – prof. dr. Roaldas Gadonas (Vilniaus universitetas, fiziniai mokslai, fizika – 02P).

Disertacija ginama Vilniaus universiteto Fizikos mokslo krypties taryboje:

Pirmininkas – prof. habil. dr. Valdas Sirutkaitis (Vilniaus universitetas, fiziniai mokslai, fizika – 02P).

Nariai:

- dr. Justinas Čeponkus (Vilniaus universitetas, fiziniai mokslai, fizika – 02P);
- prof. habil. dr. Juozas Vidas Gražulevičius (Kauno technologijos universitetas, fiziniai mokslai, chemija – 03P);
- prof. Janis Spigulis (Latvijos universitetas, fiziniai mokslai, fizika – 02P);
- dr. Roland Tomašiūnas (Vilniaus universitetas, fiziniai mokslai, fizika – 02P).

Disertacija bus ginama viešame Fizikos mokslo krypties tarybos posėdyje 2016 m. rugsėjo mėn. 27 d. 15 val. Vilniaus universiteto Lazerinių tyrimų centre, 306 auditorijoje.

Adresas: Saulėtekio al. 10, Vilnius, Lietuva.

Disertacijos santrauka išsiuntinėta 2016 m. rugpjūčio mėn. 26 d.

Disertaciją galima peržiūrėti Vilniaus universiteto ir Fizinių ir technologijos mokslų centro bibliotekose bei Vilniaus universiteto interneto svetainėje adresu: www.vu.lt/lt/naujienos/ivykiu-kalendorius.

Contents

Introduction	7
Novelty	8
Practical Value	8
Statements to Defend	9
Approbation	9
Contribution of the Authors	12
Structure of the Thesis	13
1 The Overview of the Direct Laser Writing	14
1.1 Principles of DLW	14
1.2 Polymerization Initiation Mechanisms	15
1.3 Photo-Initiators: Importance, Advantages and Disadvantages	16
2 Methods	17
2.1 Materials Used in the Dissertation	17
2.2 Preparation and Development of the Samples	18
2.3 Optical Setups	19
3 Polarization Influence on the Spatial Resolution of Polymeric Structures	21
3.1 Theoretical Calculation	21
3.2 Experimental Investigation	24
3.3 Conclusions	25
4 Reversible Deformations of the Polymeric Structures	26
4.1 Material Investigation	26
4.2 Micromechanical Sensors	28
4.3 Diffractive-Optical Sensors	29
4.4 Composite Material Sensors	30
4.5 Conclusions	31
5 The Fabrication of Scaffolds for Tissue Engineering	32
5.1 Experimental Methods	33
5.2 Optimization of the Fabrication Parameters	33
5.3 Fabricated Scaffolds	35
5.4 <i>In Vitro</i> and <i>In Vivo</i> Experimental Results	36
5.5 Conclusions	36
6 The 3D Structuring of Polydimethylsiloxane	37
6.1 Structuring Using Ti:Sapphire Laser System	37
6.2 Structuring Using Yb:KGW Laser System	40
6.3 Polymerization Initiation Mechanisms in PDMS	40
6.4 Conclusions	41
Conclusions	42
Bibliography	44
Santrauka	50
Curriculum Vitae	51

List of Abbreviations

Photo-initiators:

BIS – 4,4'-bis(diethylamino)benzophenone (*Sigma Aldrich*)
BISM – 4,4'-bis(dimethylamino)benzophenone (*Fluka*)
CAM – (1S)-(+)-camperchinon (*Sigma Aldrich*)
DIM – 2,2-dimethoxy-2-phenylacetophenone (*Sigma Aldrich*)
HYD – 2-hydroxy-4'-(2-hydroxyethoxy)-2-methylpropiophenone (*Sigma Aldrich*)
IRG – 2-benzyl-2-(dimethylamino)-4'-morpholinobutyrophenone (*Sigma Aldrich*)
IRG2 – 2-benzyl-2-(dimethylamino)-4'-morpholinobutyrophenone, Irgacure 369 (*Ciba*)
ISO – isopropyl-9H-thioxanthen-9-one (*Sigma Aldrich*)
PHE – phenylbis (2,4,6-trimethylbenzoyl)-phosphine oxide (*Sigma Aldrich*)
THIO – thioxanthen-9-one (*Sigma Aldrich*)
TPO – lucirin TPO (*BASF*)
TPO-L – lucirin TPO-L (*BASF*)

Other abbreviations:

CAD – computer-aided design
CCD – charge-coupled device
DLW – direct laser writing
DOE – diffractive optical element
ECM – extracellular matrix
FWHM – full width at half maximum
IFV – infinite field of view
In vitro – in an artificial environment outside a living organism
In vivo – within a living organism
LBO – lithium triborate
MAPTMS – methacryloxypropyltrimethoxysilane
NA – numerical aperture
Ormocer – organically modified ceramics
Ormosil – organically modified silica
PDMS – polydimethylsiloxane
PEG – poly(ethylene glycol)
PEG-DA – poly(ethylene glycol)diacrylate
PEN – 4-methyl-2-pentanone
PETA – pentaerythritol triacrylate
PGMEA – propylene glycol methyl ether acetate
PI – photo-initiator
PSF – point spread function
SEM – scanning electron microscope
SR368 – tris(2-acryloxyethyl) isocyanurate
THF – tetrahydrofuran

Introduction

Direct laser writing (DLW) in transparent cross-linkable materials is currently one of the most promising technologies used for the free-form 3D micro-structuring of pre-polymers. The first scientific paper introducing this method appeared in 1997 [1] and a very rapid development has been seen since. It was predetermined by such attributes as great flexibility in the choice of processable materials, geometry and scaling. The latter not only allows the creation of very small three-dimensional structures having repeatable spatial resolution of less than 100 nm [2], but also the high-speed production of millimeter-scale micro-structured three-dimensional objects [3,4]. The DLW structured micro-constructs are widely used in micro-optics, photonics, micro-fluidic chips, tissue engineering and many other areas [5–12].

Due to the extremely wide spectrum of applications, further development of this technology has branched in many different directions – from the record achieving improvement of resolution, relevant in areas such as photonics, to the search of new technological solutions for the rapid fabrication of a large number of macro-sized scaffolds still maintaining the micro-structure needed in tissue engineering. These and other totally different applications are united in their interest in the research of materials, however, even here their focus is different. One might need a better understanding of the resolution-influencing effects in certain materials, another would appreciate the discovery of a new laser-structurable material boasting of all the required properties according to their specific needs.

Having gained a sufficient understanding about the used polymeric materials and their properties, new areas of applications open up. At the same time, a need for further functionalizing or the combining of the properties of several materials arises. This is how the concept of *smart materials*, referring to substances which react to external stimuli, started to emerge in the scientific community, even in the field of DLW [13,14]. Such materials and their use open up the way for the development of a new generation of sensors.

No matter what applications we have in mind it is important to remember that the mere knowledge about which material has the most suitable properties for us is not enough. We can only succeed in our goals if we manage to master the DLW technique and understand the underlying physics, which means being able to correctly choose the radiation parameters and structuring algorithms for *specific pre-polymers*. That is the ultimate factor in determining the achievable fabrication efficiency, spatial resolution, the properties of the acquired structures and their suitability for certain applications.

The main **aim of the work** was to further the development of DLW in transparent cross-linkable materials paying particular attention to the fabrication peculiarities of various polymer precursors. One of the set goals was to use the obtained knowledge for the fabrication of functional materials. A new method to tune the

spatial resolution and aspect ratio of the fabricated elements was investigated, and the importance of the selection of pre-polymer not only in terms of the ease of its processing but also in terms of end-user applications was revealed. Also, a lot of attention was focused to the possibility to extend the functionality of the materials by combination of several pre-polymers in one structure.

Novelty

1. The lateral spatial resolution dependence on the angle between the laser beam's polarization vector and sample translation direction for the structures, fabricated by DLW method, was determined. A possibility to use it for tuning the aspect ratio in the SZ2080 pre-polymer was demonstrated.
2. The reversible deformations of various pre-polymers in solvents were investigated. The effect was used for the fabrication of the micro-sensors capable to feel the change of the surrounding liquid or its composition.
3. The possibility to combine more than two pre-polymers in one structure during separate fabrication stages was demonstrated as well as 3D structuring of composite objects was performed. This method was used for the creation of the solvent-sensitive bi-polymeric sensors.
4. Using SZ2080 pre-polymer a sufficient 3D fabrication throughput for the fabrication of a large number of constructs of millimeter-scale for statistical analysis was achieved. 3D micro-structured polymeric scaffolds fabricated by DLW method were used for the tissue regeneration experiments *in vivo* for the first time.
5. A 60 times larger 3D laser fabrication throughput of polydimethylsiloxane (PDMS) doped with radical photo-initiator (PI) was demonstrated if compared to other groups' results according to our knowledge. Also, for the first time laser structuring of pure PDMS without any additives was reported.

Practical Value

The experiments carried out during the preparation of this Thesis are valuable from the practical point of view in several aspects:

1. The determined dependence of the structure's lateral spatial resolution on the laser radiation's polarization opened up a new way to tune the aspect ratio of the fabricated elements by controlling the polarization direction.
2. The proposed method of fabricating composite structures by combining several pre-polymers in one object during separate fabrication stages provides the means to overcome the limitations of some of the pre-polymers. Such method may speed up the fabrication of certain structures as well as grant them additional functionality.
3. The possibility to use reversible deformations occurring in polymeric structures when they are put in different solvents to construct micro-sensors was demonstrated.

4. A non-disputable practical value was achieved by the optimization of fabrication parameters of scaffolds for tissue engineering which was demonstrated by successful use the fabricated constructs for the cartilage tissue regeneration studies *in vivo*. The positive results prompted the further development of this field towards clinical trials.
5. The throughput of the 3D laser structuring of PDMS was improved.

Statements to Defend

1. Due to the depolarization of a linearly polarized beam when focusing with a lens of high numeric aperture ($NA > 1.35$), the lateral spatial resolution of the structures fabricated out of SZ2080 pre-polymer is up to 20% higher if the polarization vector coincides with the sample translation direction, as compared to when the angle between them is 90° ; the direction of the polarization vector does not influence the axial resolution. The same dependence of lateral resolution on the polarization also appears in OrmoComp and PETA pre-polymers. The highest lateral resolution in the aforementioned pre-polymers if all other fabrication parameters are kept constant is acquired using circular polarization.
2. Structures of sparse polymeric mesh with lateral dimensions not exceeding $1.5 \mu\text{m}$ undergo reversible deformations (swelling or shrinking) in liquid environment, which can be used for the fabrication of micro-manipulators, sensors or other active objects in the micro-scale.
3. Direct laser writing can be used to fabricate micro-structured objects (structural elements in the range of $10\text{--}20 \mu\text{m}$) with 3D throughput reaching $51300 \mu\text{m}^3/\text{s}$ out of SZ2080 pre-polymer doped with IRG photo-initiator and $16400 \mu\text{m}^3/\text{s}$ throughput out of pure SZ2080; it is sufficient for the fabrication of scaffolds for statistical tissue regeneration experiments *in vivo*.
4. Yb:KGW laser system ($\lambda = 515 \text{ nm}$, $\tau = 300 \text{ fs}$, $\nu = 200 \text{ kHz}$) can be employed to fabricate 3D structures out of biocompatible elastomer PDMS using $NA = 1.25$ objective with $180 \mu\text{m}^3/\text{s}$ throughput; for the PDMS doped with radical photo-initiator the throughput increases to $720 \mu\text{m}^3/\text{s}$.

Approbation

Scientific articles in the periodical journals with an impact factor which are included in the database of Institute for Scientific Information (ISI)

- (A1) **S. Rekštytė**, M. Malinauskas, and S. Juodkazis, Three-dimensional laser micro-sculpturing of silicone: towards bio-compatible scaffolds, *Opt. Express*, **21**(14), 17028–17041, 2013.
- (A2) R. Buividas, **S. Rekštytė**, M. Malinauskas, and S. Juodkazis, Nano-groove and 3D fabrication by controlled avalanche using femtosecond laser pulses, *Opt. Mater. Express*, **3**(10), 1674–1686, 2013.
- (A3) **S. Rekštytė**, E. Kaziulionytė, E. Balčiūnas, D. Kaškelytė, and M. Malinauskas, Direct laser fabrication of composite material 3D microstructured scaffolds, *J. Laser Micro. Nanoen.*, **9**(1), 25–30, 2014.

- (A4) J. Mačiulaitis, M. Deveikytė, **S. Rekštytė**, M. Bratchikov, A. Darinskas, A. Šimbelytė, G. Daunoras, A. Laurinavičienė, A. Laurinavičius, R. Gudas, M. Malinauskas, and R. Mačiulaitis, Preclinical study of SZ2080 material 3D microstructured scaffolds for cartilage tissue engineering made by femtosecond direct laser writing lithography, *Biofabrication*, **7**(1), 015015, 2015.
- (A5) J. Mačiulaitis, **S. Rekštytė**, A. Ūsas, V. Jankauskaitė, R. Gudas, M. Malinauskas, and R. Mačiulaitis, Characterization of tissue engineered cartilage products: Recent developments in advanced therapy, *Pharmacol. Res.*, in press, DOI: 10.1016/j.phrs.2016.02.022, 2016.
- (A6) **S. Rekštytė**, T. Jonavičius, D. Gailevičius, M. Malinauskas, V. Mizeikis, E. G. Gamaly, and S. Juodkazis, Nanoscale precision of 3D polymerization via polarization control, *Adv. Opt. Mater.*, in press, DOI: 10.1002/adom.201600155, 2016.

Conference proceedings

- (A7) **S. Rekštytė**, E. Kaziulionytė, E. Balčiūnas, D. Kaškelytė, and M. Malinauskas, Direct laser fabrication of composite material 3D microstructured scaffoldings, *Proceedings of LAMP2013 - the 6th International Congress on Laser Advanced Materials Processing*.
- (A8) **S. Rekštytė**, L. Jonušauskas, A. Žukauskas, G. Gervinskas, M. Malinauskas, and S. Juodkazis, Three-dimensional nano-structuring of polymer materials by controlled avalanche using femtosecond laser pulses, *Proc. SPIE* **8972**, 89721O, 2014.
- (A9) V. Mizeikis, **S. Rekštytė**, V. Purlys, and S. Juodkazis, Reversible deformation in hybrid organic-inorganic photoresists processed by ultrafast direct laser write technique, *Proc. SPIE* **9374**, 937408, 2015.

Other scientific papers, not directly related to the topic of this dissertation

- (B1) M. Malinauskas, G. Kiršanskė, **S. Rekštytė**, T. Jonavičius, E. Kaziulionytė, L. Jonušauskas, A. Žukauskas, R. Gadonas, and A. Piskarskas, Nanophotonic lithography: a versatile tool for manufacturing functional three-dimensional micro-/nano-objects, *Lith. J. Phys.*, **52**(4), 312–326, 2012.
- (B2) **S. Rekštytė**, A. Žukauskas, V. Purlys, Y. Gordienko, and M. Malinauskas, Direct laser writing of 3D polymer micro/nanostructures on metallic surfaces, *Appl. Surf. Sci.*, **270**, 382–387, 2013.
- (B3) **S. Rekštytė**, T. Jonavičius, and M. Malinauskas, Direct laser writing of microstructures on optically opaque and reflective surfaces, *Opt. Laser. Eng.*, **53**, 90–97, 2013.
- (B4) T. Jonavičius, **S. Rekštytė**, A. Žukauskas, and M. Malinauskas, Laser nanolithography and chemical metalization for the manufacturing of 3D metallic interconnects, *Proc. SPIE* **8970**, 89700C, 2014.
- (B5) E. Balčiūnas, L. Lukoševičius, D. Mackevičiūtė, **S. Rekštytė**, V. Rutkūnas, D. Paipulas, K. Stankevičiūtė, D. Baltriukienė, V. Bukelskienė, A.P. Piskarskas, and M. Malinauskas, Combination of thermal extrusion printing and ultrafast laser fabrication for the manufacturing of 3D composite scaffolds, *Proc. SPIE* **8972**, 89721N, 2014.

- (B6) M. Malinauskas, L. Lukoševičius, D. Mackevičiūtė, E. Balčiūnas, **S. Rekštytė**, and D. Paipulas, Multiscale 3D manufacturing: combining thermal printing with additive and subtractive direct laser writing, Proc. SPIE **9135**, 91350T, 2014.
- (B7) T. Jonavičius, **S. Rekštytė**, and M. Malinauskas, Microfabrication of 3D metallic interconnects via direct laser writing and chemical metallization, Lith. J. Phys. **54**(3), 162–169, 2014.
- (B8) M. Malinauskas, **S. Rekštytė**, L. Lukoševičius, S. Butkus, E. Balčiūnas, M. Pečiukaitytė, D. Baltriukienė, V. Bukelskienė, A. Butkevičius, P. Kucevičius, V. Rutkūnas, and S. Juodkasis, 3D microporous scaffolds manufactured via combination of fused filament fabrication and direct laser writing ablation, Micromachines, **5**(4), 839–858, 2014.
- (B9) L. Jonušauskas, **S. Rekštytė**, and M. Malinauskas, Augmentation of direct laser writing fabrication throughput for 3D structures by varying focusing conditions, Opt. Eng., **53**(12), 125102, 2014.
- (B10) M. Chatzinikolaidou, **S. Rekštytė**, P. Danilevicius, C. Pontikoglou, H. Papadaki, M. Farsari, and M. Vamvakaki, Adhesion and growth of human bone marrow mesenchymal stem cells on precise-geometry 3D organic-inorganic composite scaffolds for bone repair, Mat. Sci. Eng.-C, **48**(1), 301–309, 2015.
- (B11) M. Malinauskas, **S. Rekštytė**, T. Jonavičius, D. Gailevičius, V. Mizeikis, E. Gamaly, S. Juodkasis, Femtosecond pulsed light polarization induced effects in direct laser writing 3D nanolithography, Proc. SPIE **9736**, 973608, 2016.

Conference presentations, presented by the author

- (C1) **S. Rekštytė**, E. Balčiūnas, D. Baltriukienė, V. Rutkūnas, V. Bukelskienė, R. Gadonas, and M. Malinauskas, Direct laser fabrication of composite material 3D microstructured scaffolds, CLEO/EUROPE - IQEC 2013, Munich, Germany (May 12–16, 2013).
- (C2) **S. Rekštytė**, E. Kaziulionytė, R. Gadonas, M. Malinauskas, E. Balčiūnas, D. Baltriukienė, V. Rutkūnas, and V. Bukelskienė, Trimačių kompozitinių karkasų formavimas tiesioginio lazerinio rašymo būdu, LNFK-40, Vilnius, Lithuania (June 10–12, 2013).
- (C3) **S. Rekštytė**, L. Jonušauskas, E. Balčiūnas, A. Žukauskas, R. Gadonas, S. Juodkasis, and M. Malinauskas, Laser 3D nano-structuring of polymers containing no photo-initiators, COLA, Ischia, Italy (October 6–11, 2013).
- (C4) **S. Rekštytė**, L. Jonušauskas, and M. Malinauskas, Direct laser 3D micro/nano-structuring of non-photosensitized polymers, LON, Vilnius, Lithuania (November 21–22, 2013).
- (C5) **S. Rekštytė**, D. Mackevičiūtė, and M. Malinauskas, Direct laser fabrication of composite material 3D micro-scaffoldings, LON, Vilnius, Lithuania (November 21–22, 2013).
- (C6) **S. Rekštytė**, E. Balčiūnas, and M. Malinauskas, Ultrafast laser manufacturing of composite material 3D microstructured scaffoldings, SPIE Photonics West, San Francisco, USA (February 1–6, 2014).

- (C7) M. Malinauskas, A. Žukauskas, **S. Rekštytė**, R. Buividas, and S. Juodkazis, Three-dimensional nano-structuring of polymer materials by controlled avalanche using femtosecond laser pulses, SPIE Photonics West, San Francisco, USA (February 1–6, 2014).
- (C8) M. Malinauskas, **S. Rekštytė**, E. Balčiūnas, D. Baltriukienė, and V. Bukelskienė, Trimačių mikrodarinių formavimas lazerinės nanofotoninės litografijos būdu, Conference of Young Scientists, Vilnius, Lithuania (February 11, 2014).
- (C9) **S. Rekštytė**, and M. Malinauskas, Laser microstructuring of silicone for 3D biocompatible scaffolds, Radiation Interaction with Materials: Fundamentals and Applications 2014, Kaunas, Lithuania (May 12–15, 2014).
- (C10) **S. Rekštytė**, M. Malinauskas, and S. Juodkazis, 3D ultrafast laser microsculpturing of PDMS: towards bio-compatible scaffolds and complex microfluidic templates, LPM2014, Vilnius, Lithuania (June 17–20, 2014).
- (C11) **S. Rekštytė**, V. Mizeikis, M. Malinauskas, and R. Gadonas, Skysčių sąlygotos polimerinių mikrodarinių grįžtamosios deformacijos, LNFK-41, Vilnius, Lithuania (June 17–19, 2015).
- (C12) **S. Rekštytė**, V. Mizeikis, and M. Malinauskas, Reversible deformations of polymeric microstructures induced by changing the surrounding liquid medium, CLEO/EUROPE - EQEC 2015, Munich, Germany (June 21–25, 2015).

Contribution of the Authors

Most of the experimental research tasks were performed in the laboratories of the Laser Research Center, Vilnius University during 2012–2016. Part of the research on the topic of laser structuring of PDMS was carried out at the Nonlinear Lithography laboratory supervised by Dr. M. Farsari in IESL-FORTH research institute, Crete, Greece. Also, part of the experiments on laser polarization influence to the structuring of polymers was performed at the laboratory of Laser Lithography in Shizuoka University, Japan supervised by Prof. V. Mizeikis.

The author performed all of the presented theoretical calculations and laser structuring experiments, analyzed and interpreted the data as well as assembled optical setups needed for the optical characterization of the fabricated structures. However, it is important to acknowledge the contribution of these collaborators:

- Prof R. Gadonas supervised the PhD process and created efficient conditions for the experimental work;
- Dr. M. Malinauskas generated ideas, actively engaged in data interpretation and publication of the results;
- Dr. D. Paipulas consulted in the subjects of theoretical calculations, construction of optical systems, and other matters;
- Prof. V. Mizeikis consulted in performing the investigation of polymeric materials' deformations and polarization's influence to the structuring during the practice in Shizuoka University;
- Dr. M. Farsari provided the necessary conditions for the 3D structuring experiments of PDMS during the practice in IESL-FORTH research institute;

- Prof. S. Juodkazis took an important part in the interpretation of the possible polymerization mechanisms and in the investigation of the light polarization induced effects in the DLW structuring;
- J. Mačiulaitis performed the *in vitro* and *in vivo* investigation of the polymeric scaffolds;
- PhD student D. Gailevičius fabricated and characterized the photonic crystals;
- student T. Jonavičius contributed in the theoretical calculations of the focusing with high-aperture objectives and conducted some of the experiments during the investigation of polarization influence to laser structuring;
- students E. Kaziulionytė and D. Mackevičiūtė took part in some of the composite structure fabrication experiments.

Structure of the Thesis

The doctoral dissertation consists of six chapters:

- In Chapter 1 the reader is introduced to the principles of the DLW, the polymerization process itself and its possible mechanisms.
- Chapter 2 presents the overview of the experimental methods and equipment used in the work.
- Chapter 3 is devoted for the investigation of the influence that laser polarization has on the structuring resolution of the pre-polymers.
- In Chapter 4 the reversible deformations of DLW processed polymeric materials are presented and their use for the fabrication of micro-sensors is demonstrated. A big part of the chapter is devoted for the introduction to fabrication of the composite structures and their possible use for micro-actuation.
- Chapter 5 describes the manufacturing of the polymeric scaffolds for tissue engineering and the arising challenges.
- In Chapter 6 the structuring experiments of the PDMS using Ti:Sapphire and Yb:KGW laser systems are presented and the mechanisms responsible for its polymerization are discussed.

CHAPTER 1

The Overview of the Direct Laser Writing

1.1 Principles of DLW

Direct laser writing in transparent cross-linkable materials (a shorter term – DLW in pre-polymers – will be used further on) is based on the non-linear laser-material interaction when laser radiation of high intensity is absorbed by the pre-polymer, and polymerization and cross-linking reactions are initiated inside a very small volume of the material. The process consists of four steps (see Figure 1.1): a) the preparation of the CAD model, b) structure fabrication by illuminating the sample point-by-point in the predefined trajectory, c) sample development – washing out the non-polymerized areas and d) examination of the structure by optical or scanning electron microscopy.

A pre-polymer used in DLW generally consists of the following components: a) a compound which forms a polymer network (monomers, oligomers, and their mixtures); b) a solvent; c) a light-sensitive material which is responsible for creating the reactive particles (photo-initiator – PI – in the case of radical polymerization or photo-acid generator in the case of cationic polymerization); d) other components, such as quenchers, antioxidants and others [15]. The polymerization reaction is initiated by illuminating the pre-polymer with a focused light of specific wavelength. Then the reactive species are generated in a highly localized volume of the resist where the intensity of light is sufficient for non-linear interaction to occur. The compound then undergoes a chemical reaction during which solubility of the parts which were and were not exposed to light becomes different. For the polymerization reaction to take place a very high radiation intensity – temporal and spatial overlap of photons – is needed; thus, most often *fs* lasers are used, although it is also possible to employ DLW technique by using continuous wave [16] or nanosecond [17] lasers.

DLW in pre-polymers evolved from conventional lithographic techniques which

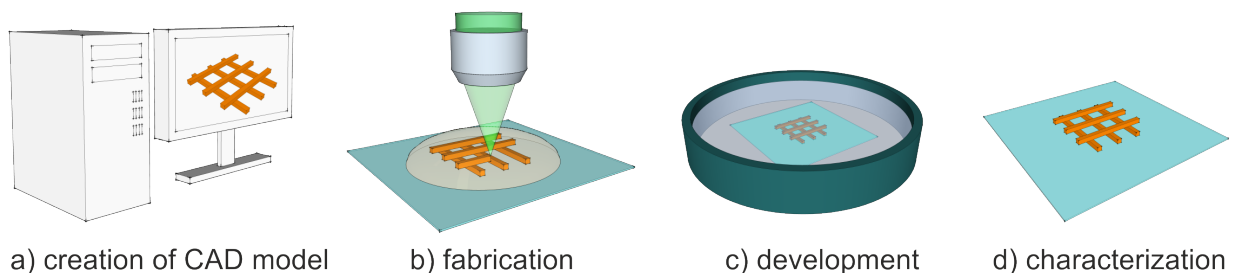


Figure 1.1: Structure fabrication steps using DLW.

were based on linear absorption. Thus, the PIs used in DLW originated there and usually have absorption spectra peaks in the UV or short-VIS region. Because of this laser radiation in the VIS or near-IR region is needed since the PIs absorb such radiation in the multi-photon manner. DLW in pre-polymers is often called *two- or multi-photon polymerization*. However, such name is not entirely correct since there is an ongoing intense scientific discussion about what mechanism is the dominant one in the laser radiation initiated polymerization [18–23]. The possible non-linear absorption mechanisms considered are multi-photon absorption and avalanche ionization. Which of them will be dominant depends on several parameters: radiation intensity, laser pulse duration, repetition rate and others.

1.2 Polymerization Initiation Mechanisms

When using ultra-short laser pulses and working near the threshold of dielectric breakdown the main polymerization initiation mechanism is direct bond breaking and in this manner generated reactive radicals [18, 24]. Mathematically it can be expressed by the rate equations of the generation of free electrons (ionization). The free electrons oscillate in the electromagnetic field of the laser pulse and during electron-lattice collisions they can be accelerated to energies exceeding the ionization potential J_i . Such electrons can cause avalanche ionization, the rate (ionization probability per second) of which is given by [25]:

$$w_{imp} \simeq \frac{\varepsilon_{osc}}{J_i} \frac{2\omega^2 \nu_{e-ph}}{(\nu_{e-ph}^2 + \omega^2)}, \quad (1.1)$$

here J_i – the ionization potential of the material, $\omega = 2\pi c/\lambda$ is the cyclic frequency of light which has a wavelength λ , and c is the speed of light. The electron quiver energy is $\varepsilon_{osc} = \frac{e^2 E^2}{4m\omega^2}$ where m and e are mass and charge of the electron, respectively, and the electric field is defined through the peak intensity as $E = \sqrt{I_p/(c\varepsilon_0 n)}$. Here ε_0 is the vacuum permittivity constant and n is the refractive index of the material. Assuming that the envelope of the beam intensity distribution is Gaussian shaped, $I_p = \frac{T \times 2P_{av}}{\nu \tau S}$, here T is the transmittance of the objective lens for the used wavelength, P_{av} is the average laser power (measured before the objective), ν – pulse repetition rate, τ – pulse duration and $S = \pi\omega_0^2$ – area of the focal spot (ω_0 – radius of the beam waist at the $1/e^2$ level). The electron-ion interaction is governed by the electron-phonon momentum exchange rate $\nu_{e-ph} \approx 6 \times 10^{14} s^{-1}$ [25]. The multi-photon absorption rate is given by:

$$w_{mpi} \simeq w n_{ph}^{3/2} \left(\frac{\varepsilon_{osc}}{2J_i} \right)^{n_{ph}}, \quad (1.2)$$

here $n_{ph} = J_i e / (\hbar\omega) + 1$ is the number of photons required for direct absorption (truncated to an integer).

These rates are used to calculate the free electron generation dynamics in order to evaluate the contribution of multi-photon and avalanche ionization to the severing of the chemical ties. The equations 1.1 and 1.2 will be used in this dissertation during the investigation of the polymerization initiation mechanisms of PDMS pre-polymer.

1.3 Photo-Initiators: Importance, Advantages and Disadvantages

As mentioned previously, photo-polymerization is usually initiated by photo-initiators which generate free radicals after excitation. In most cases they are essential for the polymerization reaction to start or at least to make it more efficient. In order to achieve an efficient polymerization reaction it is very important to choose the right PIs. They must meet several requirements. Firstly, the solubility of the photo-initiator in the pre-polymer must be taken into account. Secondly, an appropriate light absorption spectrum is essential. Also, the two-photon absorption coefficient (σ) will determine the efficiency of the laser radiation absorption. Currently, there is quite a large variety of photo-initiators to choose from, but most of them have been developed for UV lithography applications, so are not optimized for DLW. Thus their two-photon cross-sections are very small. Another very important property of the photo-initiator is its quantum efficiency (η), which shows the PI molecule's useful work – how efficiently the absorbed radiation is used for the initiation of the polymerization reaction. The photo-initiator that has low σ , but high η can be more effective in polymerization initiation than the one with high σ and low η [26].

There are several areas that suffer from the disadvantages of photo-initiators. One of them is the fabrication of optical components, since one of their main requirements is transparency at certain wavelength range (usually in the visible and near-IR). Polymerized micro-optical components suffer from the residues of photo-initiators which introduce additional absorption bands [27] thus increasing the element's optical losses and decreasing the damage threshold.

In tissue engineering applications it is very important for the used photo-initiators not to be cytotoxic. Problems may arise because of the non-reacted PIs and their products which over time break free from the polymeric mesh due to degradation. The main reason why they can be harmful is that free radicals generate reactive oxygen which can react with lipids, proteins and lead to such disruptive events like the destruction of cell membrane [28].

The most viable solution for these and other applications is to structure pre-polymers without using photo-initiators. There are several ways to achieve that:

- Using monomers mixed with a derivative which does not satisfy the usual definition of photo-initiator. Substituting ingredients can be nano-particles [29], thermal-initiators [30]; also, the mixture of several acrylates [31, 32] can be used.
- Chemical addition of certain polymerization reaction triggering derivatives, such as metal particles [33], to the monomers.
- *True* polymerization without photo-initiators when the reaction is initiated by direct bond cleavage of the monomers [19, 34].

CHAPTER 2

Methods

As mentioned previously, one of the DLW technology's strengths is a wide choice of processable materials. The first experiments on the basis of this method were carried out using acrylate pre-polymers [1]. Later commercially available epoxy resins, such as SU-8 [35] and SCR-701 [36], were employed. Further development of the DLW technology focused more on specific applications; thus, the structuring of various bio-materials, including natural (collagen [37], chitosan [38], hyaluronic acid (HA) [39], fibronectin [40], fibrinogen [40, 41], BSA [41]), synthetic (polyethylene glycol, polyamine acids and their derivatives [42]), and hybrid [38, 43] hydrogel polymer precursors, was demonstrated for applications in biomedicine. Also, in search of the universal and modifiable materials the creation of new ones is being carried out. Some examples of such substances would be hybrid organic-inorganic Ormocers (*organically modified ceramics*) and Ormosils (*organically modified silica*) which combine the properties of organic materials (strength, functionalization, processing at low temperatures) with the inorganic ones (hardness, chemical and thermal stability) [44]. Their main advantage is the ability to achieve desired chemical, optical and mechanical properties by changing the ratio of organic and inorganic components, thus adapting the material for a particular application.

2.1 Materials Used in the Dissertation

SZ2080 – a hybrid Ormosil type pre-polymer, consisting of 20% inorganic and 80% organic parts. It is optically transparent in the range of 400-2700 nm, biocompatible and distinguished by ultra-low shrinkage [27]. It is also very attractive for its fabrication properties, since it is solid (gel-like) during the fabrication allowing to freely choose the structuring trajectory.

OrmoComp – a hybrid Ormocer type material, particularly suitable for optical applications due to its high transparency in the visible and near IR range up to 350 nm. OrmoComp is also attractive for biological applications because it has the ability to attach proteins [45] and is compatible with a variety of cell lines [46].

SU-8 3025 is an epoxy pre-polymer. Contrary to other materials used in this work it undergoes cationic polymerization. Upon irradiation cationic acids are generated in the volume and the cross-linking occurs only after heating during post-bake [47]. As a result, the refractive index changes only very slightly during the fabrication which complicates real-time monitoring but is useful from the fabrication

point of view – the laser beam going through the already irradiated parts is not deflected. Also, it is solid during fabrication like SZ2080 allowing to freely choose the structuring trajectory.

PEG-DA-XXX are the derivatives of polyethylene glycol made suitable for laser processing by the addition of polymerizable acrylate groups. Here *XXX* are numbers indicating the average molecular mass of PEG-DA. They are biocompatible and biodegradable materials, very attractive for bioapplications. In this work PEG-DA-575 and PEG-DA-700 (*Sigma Aldrich*), which are known for their suitability to be structured by DLW [42, 43], were used. Both are liquid at room temperature, so selection of the fabrication algorithm is complex.

Pentaerythritol triacrylate (**PETA**) is a trifunctional acrylate polymer precursor, used mainly in the UV and electron beam curable paint, adhesive and coating industry [48]. It has been experimentally demonstrated that PETA can be structured using interference lithography [49] and DLW [21]. Like PEG-DA-XXX it is liquid at room temperature.

Tris(2-acryloxyethyl) isocyanurate (**SR368**) – another acrylate material often used as one of the components in pre-polymers, providing strength to the formed structure [50, 51]. It is solid at room temperature, so must be heated before laser processing to become liquid. This leads to a disadvantage – SR368 must be processed and developed within about an hour as later the material begins to harden and becomes unsuitable.

Polydimethylsiloxane (**PDMS**) is a silicon based organic polymer known for its elasticity [52], chemical inertness [53], thermal stability [54], gas permeability [55]. It is also relatively cheap [56], biocompatible [57] as well as optically transparent in the visible spectral range [58]. PDMS is widely used for the prototyping of the microfluidic chips, especially for biological applications [59, 60]. It is usually processed by the means of soft lithography technique, when it is mixed with a curing agent, poured over the negative template and cured by heating, thus creating 2.5D templates.

2.2 Preparation and Development of the Samples

Usually fabrication of the structures by DLW is done inside the drop of a pre-polymer which is spread on a cover glass. Depending on the material, some additional processing, e.g. heating, may be needed before fabrication. After the laser exposure samples are immersed in the organic solvents for 10–30 minutes and the non-polymerized parts are rinsed leaving only a free-standing polymeric structure on the glass. The preparation and development conditions used in this work are summarized in Table 2.1.

In order to characterize the resulting object as well as for most practical applications it is necessary for the structure to be well adhered to the substrate. For this reason, in particular when using organic pre-polymers, the glass substrates were coated with organosilane coupling agent which forms a strong bond between organic (pre-polymer) and inorganic (glass substrate) materials. In this work the adhesion of the polymeric structures to the substrates was improved by immersing the cover-glasses in the solution of MAPTMS and dichloromethane (1:80) for 24 hours and only then using them to prepare the samples for fabrication.

Table 2.1: The parameters of the preparation and development of pre-polymers.

Pre-polymer	Preparation for fabrication	Development
SZ2080 (+PI)	40–70–90°C (20 min each)	30 min in PEN
OrmoComp	–	30 min in PEN
SU-8 3025 ¹	95°C (10 min)	10 min in PGMEA ² (rinse in 2-propanol)
PEG-DA-XXX (+PI)	–	10 min in water (rinse in ethanol)
PETA (+PI)	–	15 min in 2-propanol
SR368 (+PI)	55°C (until it liquefies)	20 min in ethanol
PDMS	–	30 min PEN
PDMS +PI	100°C (30 min)	30 min in PEN

2.3 Optical Setups

Laser Systems

For the experiments described in this work three different laser systems were used. Their main differences were the employed laser source and the method which was used for the laser beam positioning inside the pre-polymer. Radiation parameters of all three laser systems are summarized in Table 2.2.

Yb:KGW. Most of the experiments were carried out at the Laser Research Center in Vilnius University using the Nanophotonics laboratory’s laser system (Figure 2.1). The radiation source was femtosecond Yb:KGW laser Pharos (*Light Conversion*), generating 1030 nm central wavelength and 300 fs duration pulses with the possibility to set the repetition rate in the 1 to 200 kHz range (all experiments were performed using 200 kHz). The beam polarization was controlled by a $\lambda/2$ or $\lambda/4$ wave-plates, positioned just prior the objective. The microscope system allowed real-time monitoring of the process and consisted of a 630 nm LED, a focusing objective, an imaging lens and a CCD camera. The fabrication was controlled by a 3DPoli software package [61]. The positioning of the laser beam inside the pre-polymer could be implemented in three different ways: 1) moving the sample using the linear motion stages, 2) moving the beam using galvanometric scanners or 3) combining stages with the scanners by using the IFV (*infinite field of view*) regime.

Table 2.2: Radiation parameters for the used laser systems.

No.	Active element	λ , nm	ν , Hz	τ , fs
1 (LT)	Yb:KGW	1030	200×10^3	300
2 (GR)	Ti:Sapphire	800	75×10^6	20
3 (JP)	Ti:Sapphire	800	80×10^6	100

¹The pre-polymer was spin-coated on the glass substrate.

²After fabrication a post-bake was carried out: 1 min 65° – 1 min 95°.

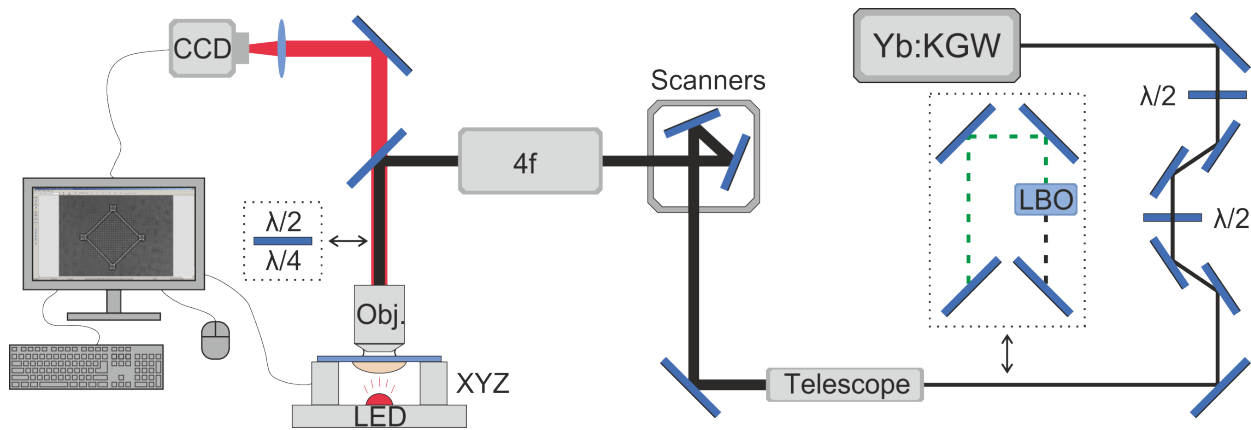


Figure 2.1: The optical setup used for DLW experiments.

Ti:Sapphire (GR). Part of the experiments described in Chapter 6 were carried out at the IESL-FORTH institute (Greece) under the supervision of Dr. M. Farsari. The radiation source was a femtosecond Ti:Sapphire oscillator Fusion (*Femtolasers*) emitting 800 nm central wavelength 20 fs duration pulses at the repetition rate of 75 MHz. Laser beam positioning inside the sample in x and y directions was carried out using galvanometric scanners while z axis and large-scale movement was performed using linear displacement tables. An objective with $NA = 1.4$ (*Zeiss*) was used for the focusing and fabrication was controlled by SAMLight (*SCAPS*) software package.

Ti:Sapphire (JP). Part of the experiments described in Chapters 3 and 4 were carried out at the Shizuoka University (Japan) under the supervision of Prof. V. Mizeikis. The radiation source was a femtosecond Ti:Sapphire oscillator MaiTai (*Spectra Physics*) emitting 800 nm central wavelength 100 fs duration pulses at the repetition rate of 80 MHz. The sample positioning was performed by high precision piezoelectric stages. For beam focusing a $NA = 1.35$ objective (*Olympus*) was used. The fabrication was controlled by 3DPoli software package.

Characterization of the Polymeric Structures for the Investigation of their Reversible Deformations

An inverted microscope type system, consisting of the xyz micrometer positioning stages for sample movement, a LED as an illumination source, a focusing objective, lens and a CCD camera, was used for the optical observation and characterization. For the observation of the diffraction patterns from the periodic polymeric structures a 633 nm wavelength HeNe laser beam was focused onto the lattices and the diffraction patterns were registered on the projection screen by a photo-camera. In both systems the illuminating/probing beam was directed at the sample, which was placed inside a glass vessel containing solvent, from the top so the level of a solvent in the container would not affect the acquired results.

CHAPTER 3

Polarization Influence on the Spatial Resolution of Polymeric Structures

Material related to this chapter was published in [A6].

The influence of laser radiation's polarization to the femtosecond processing of various materials has been widely studied. It can manifest in the formation of nano-ripples, which are mostly perpendicularly oriented in respect to the electric field vector, when surface ablation of metals [62, 63], semiconductors [62, 64], dielectrics [65, 66] or polymers [67, 68] is performed. The ablation threshold and the ablated hole's patterns are also influenced by the polarization of the beam [69].

However, scientific articles in the field of DLW in pre-polymers rarely even mention the used polarization. *S. Kawata* group showed that when forming single voxels using linearly polarized beam, they turn out elongated in the direction of the electric field vector, and when circular polarization is used, the voxels are symmetric in both x and y directions [70]. However, no in depth investigation of this effect on the fabrication of functional structures was carried out.

3.1 Theoretical Calculation

In order to understand what influence the beam polarization has on the spatial resolution of the fabricated elements it is necessary to look into the theory of focusing, especially if objectives with high NA are used, when the paraxial approximation is no longer valid. The model we used³ employs a vectorial Debye theory to calculate the point spread function (PSF) of light which is being focused through a stratified medium, in our case – immersion oil, glass substrate and pre-polymer (Figure 3.1 a). An optical system with an optical axis z is considered. In such environment the light crosses two interfaces – immersion oil/glass in the $z = -h_1$ plane and glass/pre-polymer in the $z = -h_2$. It is assumed that the layers are homogeneous and isotropic, and their refractive indices are respectively n_1 (immersion oil), n_2 (glass) and n_3 (pre-polymer). The linearly (along x direction) polarized monochromatic and coherent electromagnetic wave is emitted from a point source at $z = -\infty$. It falls onto the aperture Σ (lens) which creates a converging wave front in the image space. The

³Proposed by *P. Török* and *P. Varga* [71] and later expanded by *M.J. Nasse* and *J.C. Woehl* [72] by the addition of the lens design parameters to be suitable for more complex optical systems such as objectives.

origin of the coordinate system coincides with a corrected Gaussian focal point (the point in which the radiation would focus if all conditions would meet the objective's design parameters). The electric field is determined at the point $P(x,y,z)$ which is near the focal point. It is assumed that the size of the aperture and its distance from the point P are large compared to the wavelength. In such case the electric field components can be calculated according to these equations:

$$\begin{cases} E_x = iK(I_0 + I_2 \cos 2\phi_p), \\ E_y = iKI_2 \sin 2\phi_p, \\ E_z = 2KI_1 \cos \phi_p, \end{cases} \quad (3.1)$$

here K is a constant, ϕ_p – azimuth angle and the integrals I_0 , I_1 , I_2 are expressed as:

$$I_0 = \int_0^\alpha \sqrt{\cos \theta_1^*} \sin \theta_1 \exp[ik_0(\Psi - \Psi^*)](T_s + T_p \cos \theta_3) \times J_0(k_1 r \sin \theta_1) \exp(ik_3 z \cos \theta_3) d\theta_1, \quad (3.2)$$

$$I_1 = \int_0^\alpha \sqrt{\cos \theta_1^*} \sin \theta_1 \exp[ik_0(\Psi - \Psi^*)] T_p \sin \theta_3 \times J_1(k_1 r \sin \theta_1) \exp(ik_3 z \cos \theta_3) d\theta_1, \quad (3.3)$$

$$I_2 = \int_0^\alpha \sqrt{\cos \theta_1^*} \sin \theta_1 \exp[ik_0(\Psi - \Psi^*)](T_s - T_p \cos \theta_3) \times J_2(k_1 r \sin \theta_1) \exp(ik_3 z \cos \theta_3) d\theta_1, \quad (3.4)$$

here α – angle of the aperture ($NA = n_1 \sin(\alpha)$), $k_3 = k_0 n_3 = 2\pi n_3 / \lambda_0$ – wave-vector in the 3rd medium, λ_0 – wavelength in vacuum, J_n – Bessel function of the first type and n_{th} order, r – radial coordinate. $\sqrt{\cos(\theta_1)}$ is the apodization function. Variables with an asterisk correspond to the objective's design parameters. The aberration function Ψ for a three media system is $\Psi = -h_1 n_1 \cos \theta_1 + h_2 n_3 \cos \theta_3$ and $\Psi^* = -h_1^* n_1^* \cos \theta_1^*$ is the initial aberration function, calculated for the objective's design (when $h_2^* = 0$). T_s and T_p are transmission coefficients for s and p polarized light respectively:

$$T_{s,p} = \frac{t_{12s,p} t_{23s,p} \exp(i(\beta - \beta^*))}{1 + r_{12s,p} r_{23s,p} \exp(2i(\beta - \beta^*))}, \quad (3.5)$$

where $\beta = k_2 |h_2 - h_1| \cos \theta_2$ and $\beta^* = k_0 n_2^* |h_1^*| \cos \theta_2^*$. $t_{nn+1s,p}$ and $r_{nn+1s,p}$ are the Fresnel's transmission and reflection coefficients.

Results Figure 3.1 b)-d) shows the results of intensity distribution calculations for SZ2080 pre-polymer when the beam ($\lambda = 1030$ nm) is focused by a $NA = 1.4$ objective (performed using *Matlab* software package). Focusing of the circularly polarized beam shows a symmetrical intensity distribution (Figure 3.1 d) but for linearly polarized light it is elongated in the direction of the electric field vector (Figure 3.1 c) which can be explained by the appearance of E_y and E_z components (Figure 3.1 b), latter of which has the biggest influence to the loss of symmetry in the intensity distribution

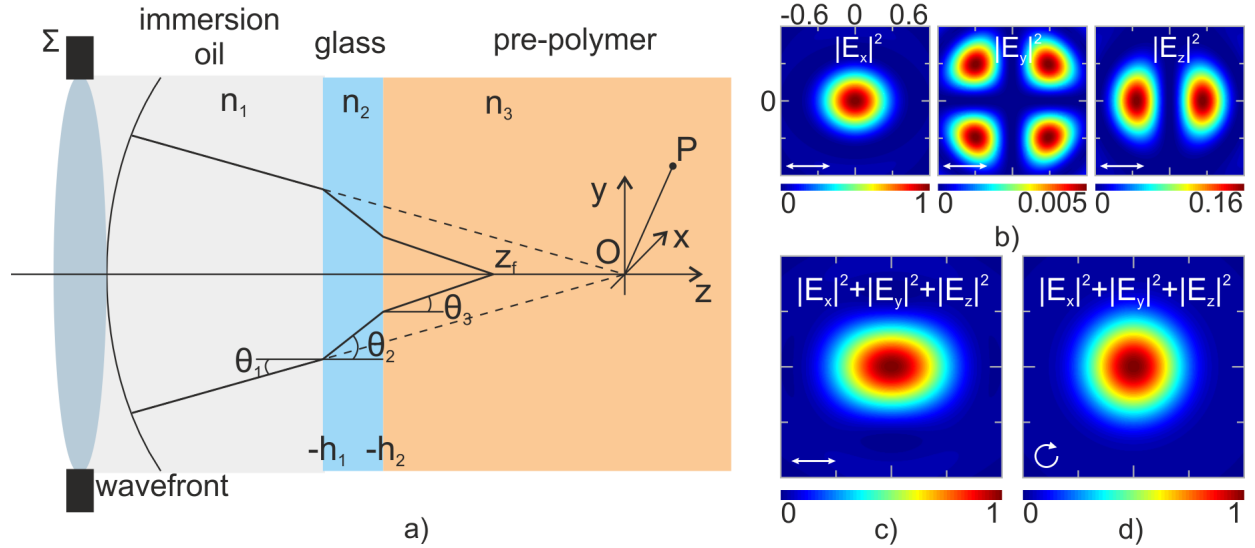


Figure 3.1: a) Focusing of the laser beam through a three-layer media. b)-d) Results of the theoretical modeling of the intensity distribution (SZ2080, $\lambda = 1030$, $NA = 1.4$, scale is in micrometers): b) separate components of the electric field and c) their sum when the focused beam is linearly polarized and d) when it is circularly polarized.

since its maximum value reaches up to 16% of the $|E_x|^2$ component. The ratios between intensity distribution profiles' FWHM values in x and y axes for different pre-polymers are given in Table 3.1. It should be noted that for circularly polarized light the FWHM value is always intermediate compared to the linear polarizations' values. It should not be expected for the ratios of fabricated lines' widths to exactly match the ones calculated theoretically as only a single point is considered when modeling, while an overlap of pulses should be taken in real-life. For correct interpretation of the line formation's dynamics an integrated intensity distribution along the sample translation direction should be considered. If the sample is translated along the electric field vector, an integrated intensity profile has higher peak power but is narrower than in the perpendicular direction. Analysis of these profiles shows that there is a point of intersection so a radiation intensity value, at which the sample regardless of its translation direction would be formed of the same width, should exist. Also, the ratio of the line widths should depend on the radiation intensity.

Table 3.1: Theoretical calculation results for various pre-polymers.

NA	λ , nm	Pre-polymer	n	z_f , μm	$\frac{FWHM_x}{FWHM_y}$	$\frac{FWHM_x}{FWHM_{aps}}$
1.35	800	SZ2080	1.504	-0.840	1.34	1.17
		SZ2080	1.504	-0.941	1.38	1.19
		SZ2080	1.504	-0.890	1.31	1.16
1.4	515	OrmoComp	1.518	-0.650	1.35	1.17
		PEG-DA-575	1.467	-1.170	1.28	1.14
		PETA	1.483	-0.990	1.24	1.12

3.2 Experimental Investigation

Structures, consisting of lines, suspended between two rigid walls (see Figure 3.2 a) and formed by changing the angle α between the polarization vector and sample translation direction ($v = 100 \mu\text{m/s}$), were fabricated. The investigation was conducted using two laser systems. Using Yb:KGW ($\tau = 300 \text{ fs}$, $\nu = 200 \text{ kHz}$, $NA = 1.4$) the pre-polymers studied were: SZ2080 without PI and doped with 1% of IRG, OrmoComp, PEG-DA-575+1% IRG, PETA+1% IRG for $\lambda = 515 \text{ nm}$ and SZ2080+1% BIS for $\lambda = 1030 \text{ nm}$. Using Ti:Sapphire (JP) ($\lambda = 800 \text{ nm}$, $\tau = 100 \text{ fs}$, $\nu = 80 \text{ MHz}$, $NA = 1.35$) the pre-polymer was SZ2080+1% BIS. The results are shown in Figure 3.2 b)-h).

Results

It was empirically found that the width of the suspended lines fabricated out of SZ2080, OrmoComp and PETA pre-polymers is greatest when the angle between the electric field vector and the sample translation direction is $\alpha = 90^\circ$ and smallest when $\alpha = 0^\circ$. This is consistent with theoretical simulations. The experiments were performed by using average laser power corresponding to the fabrication window's middle value. The investigation of SZ2080 pre-polymer using Ti:Sapphire laser system has shown the maximum difference between width of the lines reaching 20% (the average was 19%); using Yb:KGW system $\lambda = 1030 \text{ nm}$ with BIS PI – 22% (average – 22%), $\lambda = 515 \text{ nm}$ with IRG PI – 18% (average – 14%), $\lambda = 515 \text{ nm}$ without PI – 17% (average – 16%). Investigation of the OrmoComp pre-polymer showed a 5% maximum difference (average – 5%), and PETA with IRG PI – 7% (average – 7%). Furthermore, for all the investigated pre-polymers, lines fabricated using the same laser radiation parameters but circular polarization were the thinnest. In addition, after investigation of the lines' axial dimensions in SZ2080 it was discovered that the axial resolution does not depend on the angle α . In the case of circularly polarized light – also a higher resolution is achieved. Two conclusions can be made: 1) the polarization vector's direction only affects the lateral resolution of the lines and thus by changing the polarization direction it is possible to tune the structure's aspect ratio; 2) smaller lateral and axial diameters acquired using circularly polarized light can be attributed to the possibly different multi-photon absorption cross-sections for linearly and circularly polarized light.

For the PEG-DA-575 pre-polymer no clear dependence of the line's width on the angle α was observed which might be due to the material's high shrinkage, which overshadows the effect. This polymer precursor demonstrated a different sensitivity to the polarization, i.e. a change of the fabrication window (or rather the damage threshold value). Although the polymerization threshold is the same for circularly and linearly polarized light ($P_{th} = 0.08 \text{ mW}$) the damage threshold changes: for linearly polarized light when $\alpha = 0^\circ$ it is 0.90 mW , when $\alpha = 90^\circ$ it decreases to 0.24 mW and in the case of circularly polarized light it occupies the middle value – 0.58 mW .

To demonstrate the practical importance of the findings, some photonic crystals were fabricated out of SZ2080 pre-polymer. In one case, the polarization direction of the laser beam formed a 0° angle with one of the crystal's axis (thus a 90° angle with

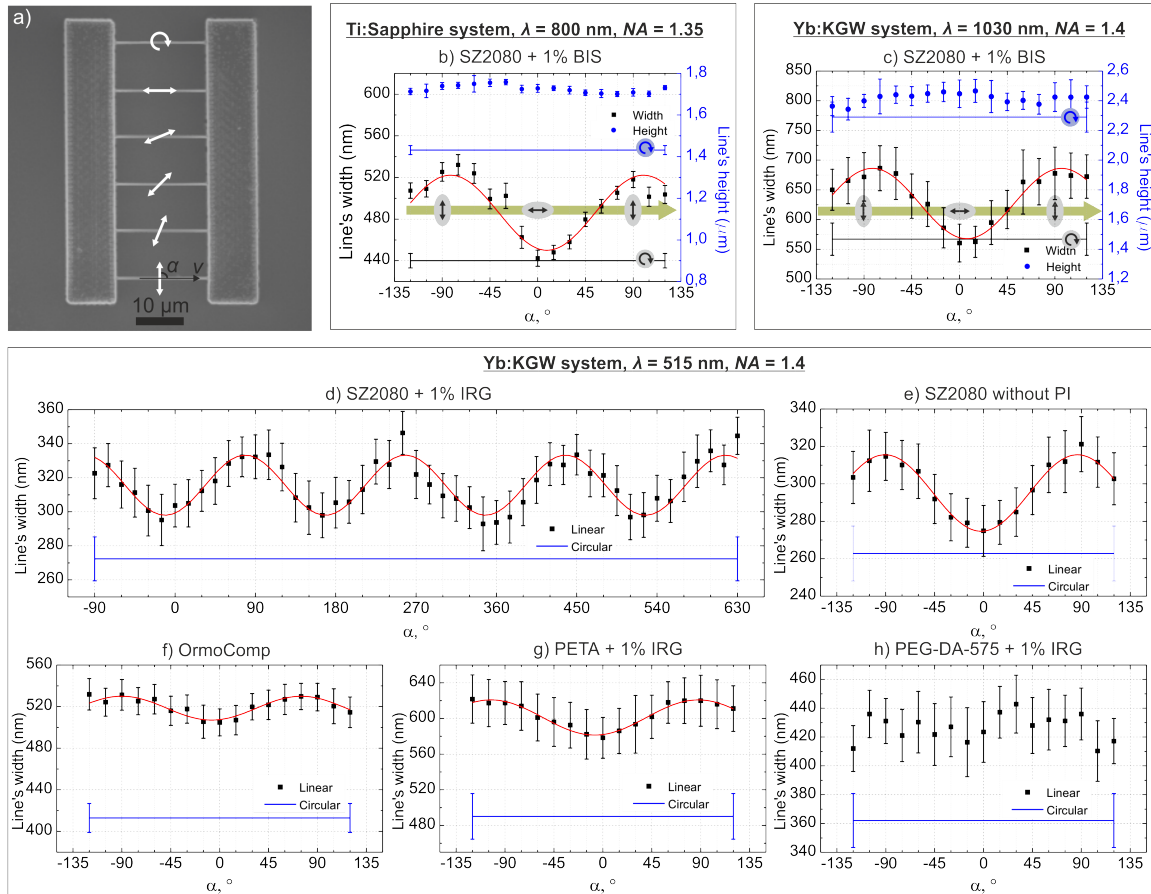


Figure 3.2: a) SEM image of a structure used for the experiments. White arrows indicate the polarization direction. b)-h) The dependence of the suspended lines' lateral and axial diameters on the angle between the electric field vector of linearly polarized beam and the sample translation direction in various pre-polymers (approximated by a $\sin(x)$ function). The error bars show the standard deviation.

another, the line width difference in respect to each other due to polarization was 8%) and in the second case it was rotated by 45° . The diffraction pattern obtained by focusing a HeNe laser beam on the first crystal was asymmetric while the second one's diffraction pattern was identical in both directions.

3.3 Conclusions

It was found that 3D suspended lines fabricated in SZ2080, OrmoComp and PETA have the smallest lateral dimensions when the angle $\alpha = 0^\circ$ and largest when $\alpha = 90^\circ$. This is consistent with theoretical modeling results obtained using the vectorial Debye theory. In PEG-DA-575 pre-polymer such dependence was not noticed, however the influence to the damage threshold was found. Also, it was discovered that line's axial resolution (at least in SZ2080) does not depend on the angle α thus polarization control may be used for dynamic tuning of the aspect ratio of the structured elements. The use of circular polarization results in the smallest lateral (for all investigated pre-polymers) and axial (at least for SZ2080) dimensions.

Reversible Deformations of the Polymeric Structures

Material related to this chapter was published in [A3, A7–A9] and presented at [C1–C7, C11, C12] conferences.

Although structures of almost any architecture may be created using the DLW in pre-polymers technique, the final product often does not completely mimic the computer model. Shape distortions of the polymeric structures arise as the material shrinks during post-development drying [73]. Although it can be used to achieve better resolution [74, 75], for most applications the shrinkage of the material is undesirable especially when structures show uneven distortions depending on the distance from the substrate to which they are attached. Photo-resists may also exhibit considerable swelling when they are immersed in solvents [74, 76]. However, this effect is less noticed and thus seldom discussed as the development process is rarely observed *in situ* and the occurring post-development shrinking while drying overshadows the swelling. If these particular polymer deformations could be utilized to our advantage, a possibility for *smart material* applications would open up. For quite awhile an idea of such *smart materials* has perked a lively interest in the scientist community. There have been demonstrations of various structures which are able to change their shape as a response to outer stimulus [77–79], yet most of the work in this area has been done in the macroscopic scale. However, a whole new range of applications become possible if we consider using DLW for the creation of such structures and consequently going to the micro-scale. There have been some reports on the DLW fabricated constructs and the use of their deformations in the solvents: a gradient structuring of a hydrogel was employed in order to achieve manipulation of a micro-sphere [80], a methacrylate based polymer was used for the fabrication of a solvent responsive micro-machine [81]. However, an in-depth study of the deformations arising in the more widely used polymers in DLW based micro-structuring has yet to be reported.

4.1 Material Investigation

The deformations which originate in 3D polymeric micro-structures fabricated out of various materials (OrmoComp, SZ2080, PEG-DA-575 and PETA, the latter three doped with 1% IRG) while they have not yet been dried out were investigated. Yb:KGW laser system was used ($\tau = 300$ fs, $\nu = 200$ kHz, $NA = 1.4$). The fabri-

cated structures were resolution bridges consisting of two rigid non-deformable walls attached to the glass substrate separated by the distance of $20\ \mu\text{m}$ which acted as a support for thin lines written using $100\ \mu\text{m/s}$ sample translation velocity and changing the average laser power over the whole fabrication window (Figure 4.1 a). Thus, thin ($<1.5\ \mu\text{m}$) lines of varying diameter were acquired. After the fabrication the samples were developed in respective developers and then immersed in different solvents – PEN, ethanol, acetone, 1- and 2-propanol or water.

The experiments showed that all of the used materials tend to swell in PEN, acetone and alcohols (only the degree of swelling differs), but the bended lines straighten up as soon as the structures are placed in water, with the exception of PEG-DA-575 which will be discussed separately. As an example we shall address what occurs in structures fabricated out of SZ2080 as shown in Figure 4.1 b), top row (the same picture can be used as a guide to what occurs in OrmoComp and PETA). During the sample's development in PEN the fabricated straight lines bend as soon as the non-polymerized material is washed away. Substitution of PEN with ethanol leaves the lines bent. However, when the structure is immersed into the water, the lines straighten up. Subsequent rinsing in 1-propanol, 2-propanol or acetone bend the lines again. Such behavior (bending and straightening) repeats itself for at least nine cycles. Also, it has been noticed that the structures remain sensitive to the surrounding medium after keeping the samples dry for extended periods of time (up to 3 weeks in ambient conditions) and then immersing them to the same solvents.

Structures fabricated out of PEG-DA-575 demonstrated slightly different behavior, because it is known to be a hydrogel type material which can efficiently absorb water. Consequently, PEG-DA-575's lines remain bent even when immersed in the water (see Figure 4.1 b), bottom row). The fact that some polymeric materials behave differently in the same solvents open up more possibilities for practical applications.

Also, no influence of the line's diameter to their behavior was noticed suggesting their sensitivity to the surrounding solvents at least as long as their lateral diameter does not exceed $1.5\ \mu\text{m}$.

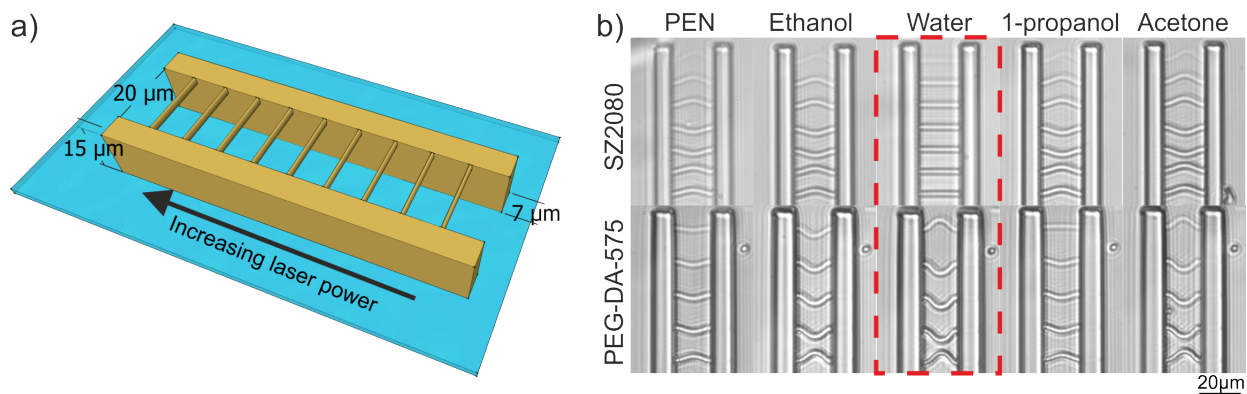


Figure 4.1: a) A CAD model of a resolution bridge and b) optical microscope images of SZ2080 and PEG-DA-575 structures in various solvents; dashed rectangle indicates different behavior.

4.2 Micromechanical Sensors

As a demonstration of the polymeric structure's sensing abilities a model of a simple micro-mechanofluidic element, which has the ability to rotate as a result of polymer's deformations, was created and then fabricated out of SZ2080. It consisted of a mechanically rigid and non-deformable lever (fabrication parameters: $P_{av} = 7$ mW, $I_p = 0.050$ TW/cm², $v = 50$ μ m/s) connected to the medium sensitive rods (lateral diameter <1 μ m, formed by 1–3 parallel scans set 0.3 μ m apart, fabrication parameters: $P_{av} = 8$ –9 mW, $I_p = 0.058$ –0.065 TW/cm², $v = 50$ μ m/s) which were anchored to the substrate (see Figure 4.2 a). The rods were designed to rotate the lever by swelling or shrinking. Structures were fabricated using the Ti:Sapphire (JP) ($\lambda = 800$ nm, $\tau = 100$ fs, $\nu = 80$ MHz, $NA = 1.35$) laser system.

The designed rotating structure has two advantages over the resolution bridges: 1) it is suitable for observing not only the swelling of the polymer but also its possible shrinking; 2) a degree of swelling/shrinking is more easily determined as it is converted into the angle of rotation, which is more obvious and easy to measure.

When the structure is placed in some kind of solvent, the rods may expand (in ethanol, Figure 4.2 b) or contract (in water, Figure 4.2 d), thus moving the lever. If the liquid is a mixture of several solvents, then depending on its volume percent (v/v%) composition the lever may occupy an intermediate position (Figure 4.2 c). Also, the experiments showed that development in PEN gave rise to the strongest rotation of the lever and subsequent immersion in ethanol reduces the rotation, however, the swelling is still clearly observed. When the structure is placed in water, the rods shrink, thus pulling the lever to the opposite direction. After investigating the rotation angles for the structures with rods fabricated using different radiation power and of different lengths (20–30 μ m) it was noticed that both of these parameters influence the degree of rotation. The longer the rods – the higher absolute deformations are achieved resulting in wider rotation angle, however too long rods may fall on the substrate and stick thus rendering the structure obsolete. Mechanical strength of the rods is also very important as very thin rods may not give out enough force to push the rigid lever. Although a rod formed by a single laser scan may deform more, it tends to bend and not push the lever during swelling, while a rod formed using 3 parallel scans is more strong mechanically and does not bend so easily. If lower laser intensity for fabrication is used, the achieved degree of cross-linking is also lower, thus the rods tend to deform more. A decrease in swelling was observed during subsequent solvent substitution.

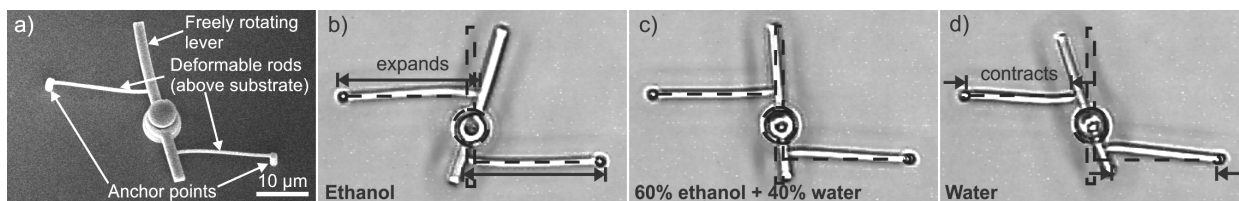


Figure 4.2: A freely rotating lever fabricated out of SZ2080 and capable of determining the composition of the solvent: a) SEM image and b)-d) optical microscope images of the actuator in action. Dashed lines show the modeled structure orientation.

4.3 Diffractive-Optical Sensors

For further study, a structure consisting of a diffractive optical element (DOE) – 3D cubic lattice (fabricated above the substrate) – and a cage used for its encapsulation so the lattice would not go adrift (see Figure 4.3 a) were fabricated. Such object could detect both the shrinking and the swelling of the material. SZ2080 pre-polymer and Yb:KGW laser system were used ($\tau = 300$ fs, $\nu = 200$ kHz, $NA = 1.4$). The DOEs were 70–72 μm wide, with a period of 3–6 μm and had three layers in z direction. The fabrication parameters were $P_{av} = 22\text{--}50$ μW ($I_p = 0.12\text{--}0.26$ TW/cm^2), $v = 100$ $\mu\text{m}/\text{s}$.

Diffraction of the HeNe beam from the DOE was measured in various solvents. The dependence of the relative change of the lattice period on the fabrication power is shown in Figure 4.3 b). The maximum deformation is observed when minimum laser power is used – in the working range (the range of power values using which the DOEs survive in all solvents) an overall 24% change in the period of the lattice is reached (–12% in water and up to +12% in PEN). By increasing the power and consequently the degree of cross-linking the deformations lessen and at 38 μW ($I_p = 0.20$ TW/cm^2) become saturated at –1% for shrinkage and 2–3% for swelling. The same trend was observed for 4–6 μm period lattices. It was also noticed that higher degree of deformations is observed in the DOEs of larger period which might be due to the fact that they have less overlapping areas (line intersections) in which the degree of cross-linking is higher.

Although the presented results were acquired using the polarization control (the electric vector was always at a 0° angle with one of the lattice’s axis), and a variation of line width’s was observed, no clear dependence of the diffraction angle on the diameter of the line was noticed. Thus, we think that the degree of cross-linking and not the dimensions of the structure have the biggest influence to the deformations.

Also, Figure 4.3 c) shows the repeatability of the deformations in the DOEs over 10 cycles of the solvent change. It can be seen that the swelling after the first few cycles decreases visibly until it stabilizes at a constant value. However, in terms of material shrinkage the results are quite different as it fluctuates around the same value and does not visibly decrease even after 10 cycles. It can be concluded that even though very high deformations are only noticeable in the first few cycles of the solvent change, they do not disappear completely, thus they do not become obsolete.

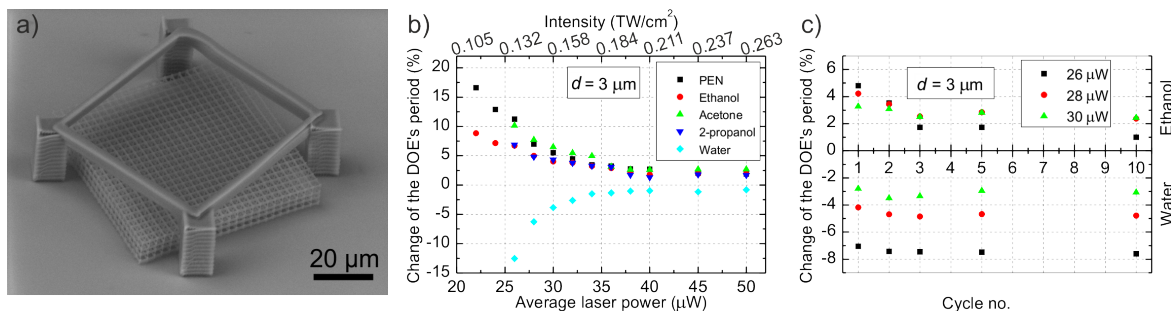


Figure 4.3: a) SEM image of the DOE and the dependence of the relative change in the period of the DOE b) on the laser power and c) the solvent change cycle number.

4.4 Composite Material Sensors

Principles of the Composite Material Structuring

From the practical point of view, more functionality of 3D polymeric structures could be achieved by combining two materials in one structure, however, not by directly mixing them, but by adding them in separate stages: fabricating a rough geometry out of one pre-polymer, developing it and then pouring over another polymer precursor and polymerizing additional elements. The first steps in combining two materials using DLW have already been taken – composite polymer scaffolds with distinct protein-binding properties were fabricated [45], and fibronectin protein at specific sites to the BSA scaffold has been added [82]. Both demonstrations were meant for biomedical applications, however, this technique may also have some advantages in areas such as micro-sensors.

The structures presented in this section were fabricated using Yb:KGW laser system ($\tau = 300$ fs, $\nu = 200$ kHz, $NA = 0.65$ – 1.4). Figure 4.4 demonstrates the versatility of the fabrication of multi-component structures. Firstly, as many as four different materials may be used, as each stage of the material preparation (e.g. heating) and development does not seem to damage the already fabricated parts (Figure 4.4 a). Also, the possibility to use the first material as a support structure for the second one is seen in Figure 4.4 b) where rigid SZ2080 walls support PDMS lines which would otherwise collapse. 3D structuring directly onto the first material without touching the substrate is also possible as shown in Figure 4.4 c). Finally, even if used materials do not stick to each other or if moving parts are needed, the structuring of completely separate objects loosely interconnected with each other can be used (Figure 4.4 d).

Fabrication of the Sensor

A structure operating similarly to a bimetallic strip (bending due to material's different response to environment) was designed (see Figure 4.5). It consisted of a rigid wall with thin rods sticking out and was fabricated out of mechanically strong SZ2080 (fabrication parameters: $P_{av} = 0.1$ mW, $I_p = 0.53$ TW/cm², $v = 100$ μ m/s). After photo-structuring was performed, the sample was developed in PEN, PEG-DA-575 was poured over the structure and a layer of the hydrogel was polymerized to the side of the SZ2080 rods (fabrication parameters: $P_{av} = 0.15$ mW, $I_p = 0.79$ TW/cm², $v = 50$ μ m/s).

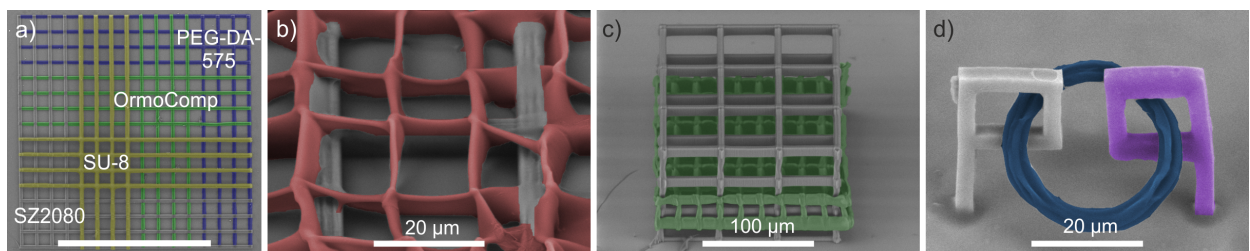


Figure 4.4: SEM images of multi-component structures. Color coding: SZ2080 – gray, SU-8 – yellow, OrmoComp – green, PEG-DA-XXX – blue, PDMS – red, SR368 – purple.

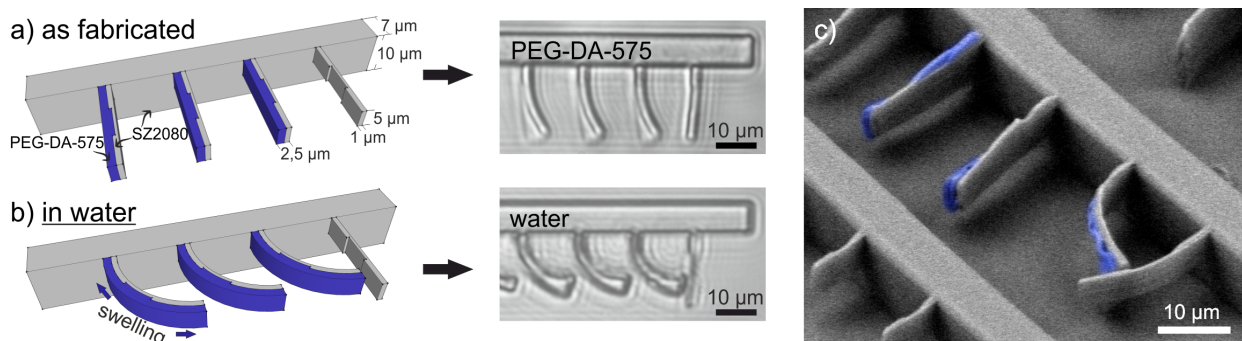


Figure 4.5: A composite structure's CAD model and optical microscope images a) as fabricated (after the addition of PEG-DA-575 layer, before development) and b) in water. In the CAD model SZ2080 is colored gray and PEG-DA-575 – blue. c) SEM image of the structure (for clarity the PEG-DA-575 is colored blue).

Various approaches to the composite structure's fabrication were tested – from the addition of PEG-DA-575's layer only at the center part of the rod, to its full coverage, and the best results were acquired with the latter. The fabricated structure in action is shown in Figure 4.5 a)-b). It consists of four rods fabricated out of SZ2080, three of which have a hydrogel layer attached on one side (the fourth rod is used as a reference to compare how the structure's behavior depends on its composition). During the addition of the PEG-DA-575 layer the laser beam is being scanned along the rod and the growth of polymeric mesh results in a slight movement of the thin structure. Thus, a slight bending is observed just after the fabrication (see Figure 4.5 a) optical microscope image). After development in water the PEG-DA-575 layer swells, while SZ2080 shrinks. This results in a large bend towards the reference rod (Figure 4.5 b). The same behavior repeats itself during the subsequent solvent change cycles. Also, a dependence of the degree of bending on the solvent was noticed – the rods showed a smaller bending when immersed in ethanol as compared to water. SEM images of the structure show that the rods are mechanically stable, do not sag with the addition of another material and straighten up after drying (see Figure 4.5 c). It should be taken in account that direct contact between the separate polymeric parts (e.g. two rods) should be avoided, as it may result in them sticking together and becoming obsolete.

4.5 Conclusions

Our observations show that the degree of deformations, occurring when DLW fabricated structures are placed in various solvents, can be controlled by changing the surrounding liquid medium or its composition. Such micro-structures are distinguished by their momentarily response to the environmental changes, deformations have repeatable nature (for at least 10 liquid change cycles) and are not restricted to the non-dried-out samples. This makes them applicable as environmental sensors, mechanical actuators in micro-fluidic templates, tunable DOE elements and in other areas. The functionality of such sensors may be expanded by using multi-component structures.

CHAPTER 5

The Fabrication of Scaffolds for Tissue Engineering

Material related to this chapter was published in [A4, A5] and presented at [C8] conference.

Since the ancient times a possibility to regrow a tissue, body part or even to create a whole human body out of nothing has peaked people's imagination. So it is not surprising that the ideas from myths and fairy tales began to move into reality creating the science of tissue engineering, which is now being increasingly used to help people return to normal life after an accident. The term *tissue engineering* was mentioned for the first time in 1984 [83], while its definition can be found in the article by *R. Langer* and *J. Vacanti* in the journal *Science* [84]:

tissue engineering is an interdisciplinary field that applies the principles of engineering and the life sciences toward the development of biological substitutes that restore, maintain, or improve tissue function.

The first steps towards tissue engineering were made hundreds years BC in two different directions. The engineers crafted simple prosthetics used after losing a limb, while the medics developed the skin grafting procedures. For tissue engineering, however, both these fields had to be combined. In order to understand how engineering of the tissue is performed we must understand what constitutes a tissue. There are two main components: the cells and the extracellular matrix (ECM) – the secretion product of the cells that is in dynamic equilibrium with them. It follows that the best scaffold for artificial tissue would be the ECM or a structure which replicates it, however, due to its complex architecture it is not a trivial task to make such construct, thus, it is usually settled for structures which meet the following demands [85]:

- the architecture ensures sufficient porosity for the growth of new tissue, material transport and vascularization;
- the materials are biologically compatible (non-toxic) with the grown cells;
- the mechanical properties of the materials used for the scaffold match tissue's native properties.

DLW is a promising technology for the scaffold fabrication due to its wide range of processable materials, tunable resolution over a wide range, full control over the architecture and even the possibility to work in the environment of live tissue [86]. Synthetic polymers are often used for the scaffold fabrication since natural ones usually lack the required mechanical stability. If there is a requirement that the

scaffold should degrade in time and leave only the newly formed tissue, biodegradable materials should be used. If the main goal is a study of the scaffold geometry's influence on the cell behavior, then non degrading ones can be used. This includes already widely used for DLW Ormocers, Ormosils, epoxies and acrylates some of which have been studied and found to be biocompatible [3, 46, 87, 88].

Although the scaffolds fabricated using DLW have been quite extensively studied for tissue engineering applications [51, 89, 90] *in vitro*, their *in vivo* capabilities have not yet been reported.

5.1 Experimental Methods

The chosen material was SZ2080 pre-polymer known to be biocompatible [3] and also suitable for structuring without the use of photo-initiators [19]. The latter property allows to perform the PI's toxicity studies when the non-degradable 3D constructs are used for tissue regeneration. The objective used was $NA = 0.8$ (*Zeiss*) and the IFV regime was employed. The sample was prepared by 2–3 consequent heatings on the hot-plate to achieve the height of pre-polymer drop larger than 200 μm while its area had to be $\approx 1.5 \times 1.5 \text{ cm}^2$. This was needed due to the height of scaffolds (around 200 μm) and their lateral size (several mm, at least 10 scaffolds were fabricated on the same substrate). The development of the samples was also longer than usual – scaffolds were left in the developer for an hour, then moved to a clean one and left for several hours. The procedure was repeated at least two more times with a couple of hours time span in between the solvent change.

Since the scaffolds were fabricated for the eventual use in *in vivo* experiments, they were not stuck to the glass substrate, thus, for the ease of handling during the sample characterization, one scaffold was always fabricated on the substrate.

5.2 Optimization of the Fabrication Parameters

For statistical investigation a high number of scaffolds is needed; thus, the optimization of fabrication parameters is critical. The aim of this task is to find the set of fabrication parameters (such as lateral and axial hatching distances d_{xy} and d_z , sample translation velocity v , average laser power P_{av}) that ensures high-quality structures (without visible deformations) and high throughput (calculated as polymerized volume in time V_{pol}/t). Three main factors influence the achievable throughput.

Material properties. The main problem arises if the pre-polymer is liquid during fabrication as it moves due to inertia. This limitation can be overcome by using the galvanometric scanners and not linear stages for the fabrication. Also, each pre-polymer has its "suitability" for the DLW processing – some are easily structured, have wide fabrication windows and others are much more difficult to use.

Hardware and software limitations. Hardware limitations can manifest themselves by the limited fabrication area (for piezoelectric stages and galvanometric scanners), velocity (for piezoelectric stages), shutter closing delay or high inertia (in the case of linear motion stages such as *Aerotech*). The latter manifests by the separation of lines formed by parallel scans, their curvature; however, in some cases

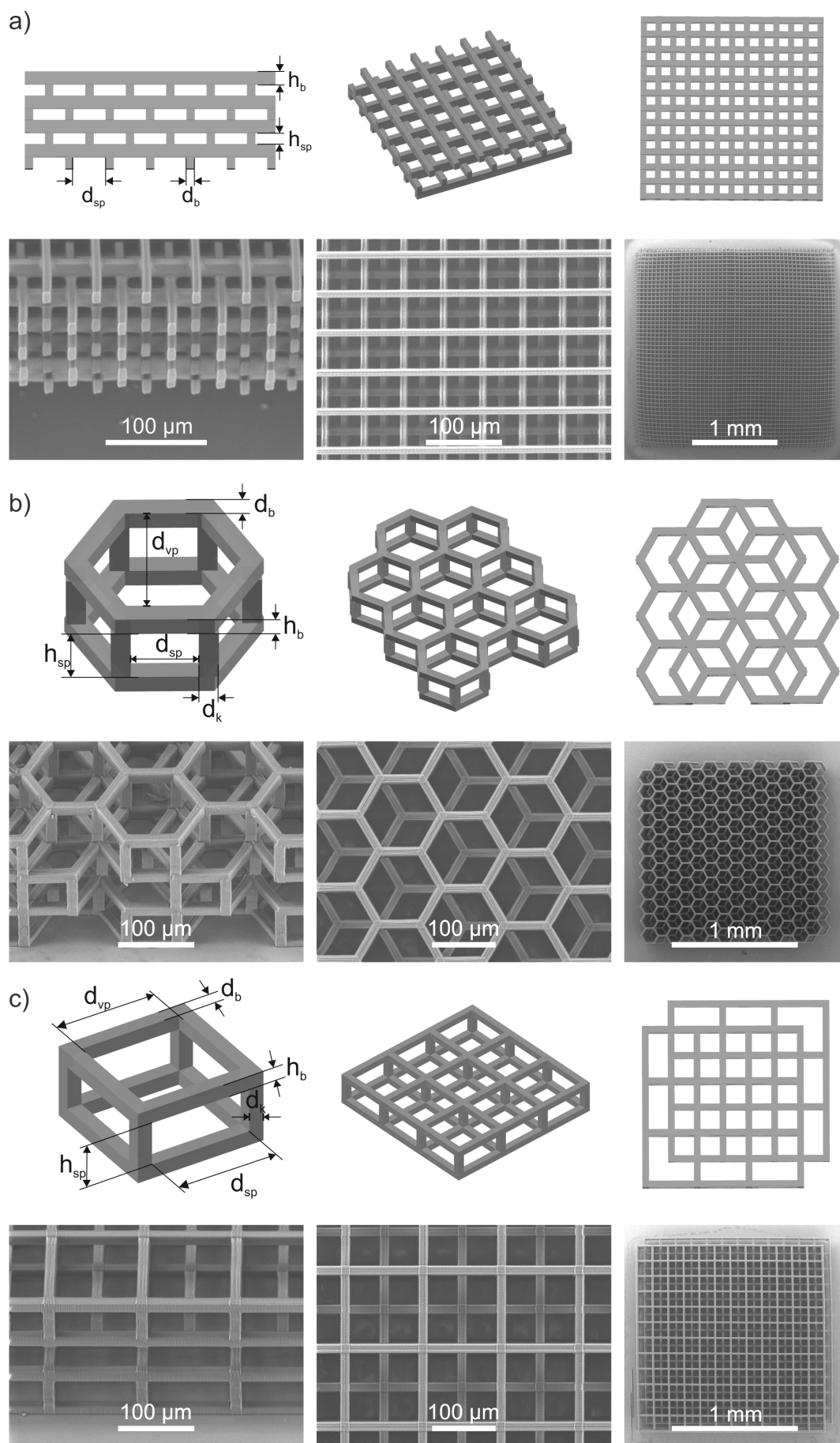


Figure 5.1: CAD models and SEM images of the fabricated scaffolds of the a) wood-pile, b) hexagonal and c) rectangular types.

they can be overcome by the use of IFV regime. Software limitations arise if large (mm-cm scale) scaffolds having complex geometry are fabricated as the computer resources needed for the code generation may not be sufficient.

Geometry of the scaffold. The more complex it is, the lower beam scanning velocity must be used even when using IFV regime. This means that the throughput of a simple rectangular scaffold will always be higher than that of a hexagonal.

5.3 Fabricated Scaffolds

Woodpile type scaffold consisted of 10 μm wide and 15 μm high logs arranged in 50 μm period (Figure 5.1 a). Each layer was at 90° angle in respect to the preceding layer. Every second layer was shifted by half a period. In z direction the scaffold consisted of seventeen layers.

Hexagonal type scaffold was composed of hexagonal cells pervious in all directions (Figure 5.1 b). The apothem of a hexagon was 50 μm , the side hole height was 45–55 μm and width 51 μm . Each layer of such cells was shifted in one direction in respect of the previous layer. The rod's height and width was tuned in the range 10–15 μm . In z direction each scaffold consisted of three layers.

Rectangular type scaffolds were made up of rectangular cells which, in the case of hexagonal, were pervious in all directions (Figure 5.1 c). The width and height of the rods was 15 μm , the upper pore size was $105 \times 105 \mu\text{m}^2$, and the side pore – $105 \times 45 \mu\text{m}^2$. Each layer of the cells was shifted in both (x and y) directions by half a period. In z direction each scaffold consisted of three layers.

Although the first experiments were performed using woodpile and hexagonal type scaffolds (their size was up to $2.1 \times 2.1 \times 0.21 \mu\text{m}^3$) only the latter showed promising results after initial tests with cells, so the woodpile type was dismissed.

As the DLW method is especially suitable to fabricate scaffolds with controlled architecture hexagonal and rectangular type scaffolds with similar parameters were fabricated for the evaluation of the geometry's influence to cells. Since it is not possible to make all parameters the same, the following were chosen:

- area of the top pore orifice (as seen through the whole scaffold) $\approx 2090 \mu\text{m}^2$;
- top pore size (of one cell) $d_{vp} \approx 100 \mu\text{m}$;
- porosity $>85\%$;
- the lowest pore size (in any direction) of the side pore $h_{sp} \approx 45 \mu\text{m}$;
- equal width and height of the rods ($h_b = d_b = d_k = 15 \mu\text{m}$).

The optimal parameters for these scaffolds using SZ2080+1% IRG were as follows.

Table 5.1: The parameters for some of the fabricated scaffolds.

Scaffold type	Porosity, %	Size, μm^3	Fabrication duration, min.	Throughput, $\mu\text{m}^3/\text{s}$
Hexagonal	87	$1581 \times 1525 \times 195$	37	27500
Rectangular	89	$1515 \times 1515 \times 195$	16	51300
Rectangular ^{without PI}	89	$1515 \times 1515 \times 195$	50	16400

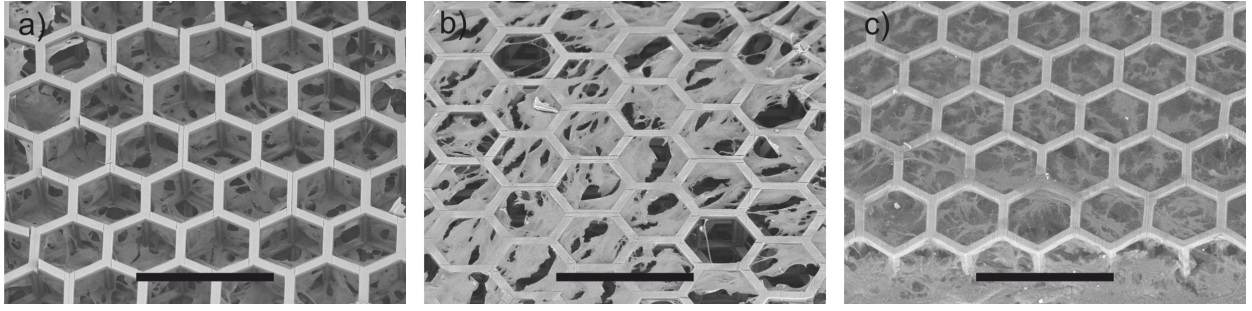


Figure 5.2: Hexagonal type scaffolds seeded with chondrocytes incubated for a) 3, b) 7 and c) 14 days. Scale bar – 200 μm .

For both (hexagonal and rectangular) types the same hatching distance $d_{xy} = 0.5 \mu\text{m}$ and $d_z = 7.5 \mu\text{m}$ and same beam scanning velocity for the vertical rods – $v_k = 6 \text{ mm/s}$ – was used. The beam scanning velocity for the horizontal rods was $v_b = 15 \text{ mm/s}$ and 10 mm/s for the rectangular and hexagonal scaffolds, respectively. Also, rectangular type scaffolds were fabricated out of SZ2080 without photo-initiator. The achieved throughput was lower than for the doped pre-polymer due to the difference in the spatial resolution achievable in both cases. The optimal parameters were: $d_{xy} = 0.4 \mu\text{m}$, $d_{z_b} = 4.5 \mu\text{m}$, $d_{z_k} = 7 \mu\text{m}$, $v_k = 5 \text{ mm/s}$, $v_b = 8 \text{ mm/s}$. The typical sizes and throughputs of the fabricated scaffolds are summarized in Table 5.1.

5.4 *In Vitro* and *In Vivo* Experimental Results

In collaboration with the Lithuanian University of Health Sciences the fabricated scaffolds were used for the pre-clinical tests of cartilage regeneration. The isolated rabbit allogenic chondrocytes seeded on the hexagon shaped scaffolds showed penetration to the interior, their distribution in the inside pores increased steadily over 14 day period. Immunohistochemical study also showed the formation of ECM. The scaffolds were implanted into the rabbits' knee defects and during the observations after 1, 3 and 6 months no unusual inflammation was noticed. Also, better results in cartilage regeneration were achieved using the DLW fabricated constructs than commercial collagen membranes.

5.5 Conclusions

Limiting factors for rapid large scale fabrication of scaffolds for tissue engineering were discussed. Using the SZ2080 pre-polymer doped with IRG photo-initiator, constructs reaching up to $2.1 \times 2.1 \times 0.21 \text{ mm}^3$ in size for cartilage regeneration were fabricated. The fabrication of hexagonal type constructs reached $27500 \mu\text{m}^3/\text{s}$, throughput while for the rectangular type – $51300 \mu\text{m}^3/\text{s}$. Also, pure SZ2080 was used for rectangular type scaffold fabrication reaching 3D throughput of $16400 \mu\text{m}^3/\text{s}$. The *in vitro* experiments of cell growth in hexagonal type scaffolds demonstrated positive results, and first *in vivo* investigation of DLW structured scaffolds showed that such constructs regenerate the cartilage tissue better than commercial collagen membranes.

CHAPTER 6

The 3D Structuring of Polydimethylsiloxane

Material related to this chapter was published in [A1, A2, A8] and presented at [C3, C4, C7, C9, C10] conferences.

SZ2080 pre-polymer, which is suitable for various tough tissue (bone, cartilage) regeneration experiments due to its mechanical properties, was used for the fabrication of scaffolds described in the previous chapter. However, for soft tissues (muscles, blood vessels) it is too rigid and other materials, such as polydimethylsiloxane (PDMS), should be considered. It is attractive not only for its biocompatibility, but also for the possibility to tune its elastic modulus from a few kPa up to several MPa [91] – the range which is suitable for most of the soft tissues [92]. There have been some reports on 3D laser structuring of PDMS using photo-initiators [93–95] and fabrication of a suspended line using a curing agent [30]. However, the achieved 3D structuring throughput ($\approx 12 \mu\text{m}^3/\text{s}$) is too small for practical use, especially if large-scale structures, such as scaffolds, are needed.

In this chapter a study on the laser structuring of the pure PDMS and doped with various PIs will be presented. For the experiments a commercial elastomeric PDMS kit Sylgard 184 (*Dow Corning*) was used. The pre-polymer was doped with various photo-initiators in the following way: the PI's were dissolved in tetrahydrofuran (THF), then added to the PDMS and left stirring for an hour in the closed bottle. Afterwards the bottle's cap was taken off and the mixture left to stir for another 12 hours for the THF to evaporate. Since it did not evaporate completely even after such time, the samples were heated for 30 min at $\approx 100^\circ\text{C}$ before laser structuring.

The experiments were carried out using Ti:Sapphire (GR) ($\lambda = 800 \text{ nm}$, $\tau = 20 \text{ fs}$, $\nu = 75 \text{ MHz}$, $NA = 1.4$ (*Zeiss*)) and Yb:KGW ($\lambda = 515 \text{ nm}$, $\tau = 300 \text{ fs}$, $\nu = 200 \text{ kHz}$, $NA = 1.25$ (*Olympus*)) laser systems. Fabrication throughput within the bounds of this investigation is defined as the polymerized volume over time unit calculated as $dx \times dy \times dz \times v$ where the variables dx , dy and v are those, with which structures corresponding to the model without visible defects are acquired.

6.1 Structuring Using Ti:Sapphire Laser System

The study was performed in four stages:

1. *Investigation of the PIs' suitability for laser structuring of PDMS.* 12 different photo-initiators were used to prepare PDMS mixtures with 0.5% PI (see Table 6.1).

Table 6.1: The results of the structuring experiments of PDMS using Ti:Sapphire ($\lambda = 800$ nm, $\tau = 20$ fs, $\nu = 75$ MHz) and Yb:KGW ($\lambda = 515$ nm, $\tau = 300$ fs, $\nu = 200$ kHz) laser systems.

Laser system	No.	PI	PI concentration %	Mixture is homogenic		Observable polymerization		Survives the development		3D throughput, $\mu\text{m}^3/\text{s}$
				Yes(+)	No(-)	Yes(+)	No(-)	Yes(+)	No(-)	
Ti:Sapphire	1	IRG	0.5 (1)	+	(-)	+		+		
	2	BISM	0.2 (0.5)	+	(-)	+		-		
	3	THIO	0.2 (0.5)	+	(-)	+		+		
	4	IRG2	0.5	-		-		-		
	5	BIS	0.5	-		-		-		
	6	ISO	0.5 (1) [1.5]	+	(+)	+	(+)	+	(+)	(20)
	7	TPO	0.5 (1) [1.5]	+	(+)	+	(+)	-	(-)	
	8	TPO-L	0.5 (1) [1.5]	+	(+)	+	(+)	-	(-)	
	9	HYD	0.5	-		-		-		
	10	PHE	0.5	-		-		-		
	11	CAM	0.5	+		+		-		
	12	DIM	0.5	+		+		-		
	13	-	-	-		+		-		
Yb:KGW	3	THIO	0.2	+		+		+		180
	6	ISO	0.5	+		+		+		720
	13	-	-	+		+		+		180

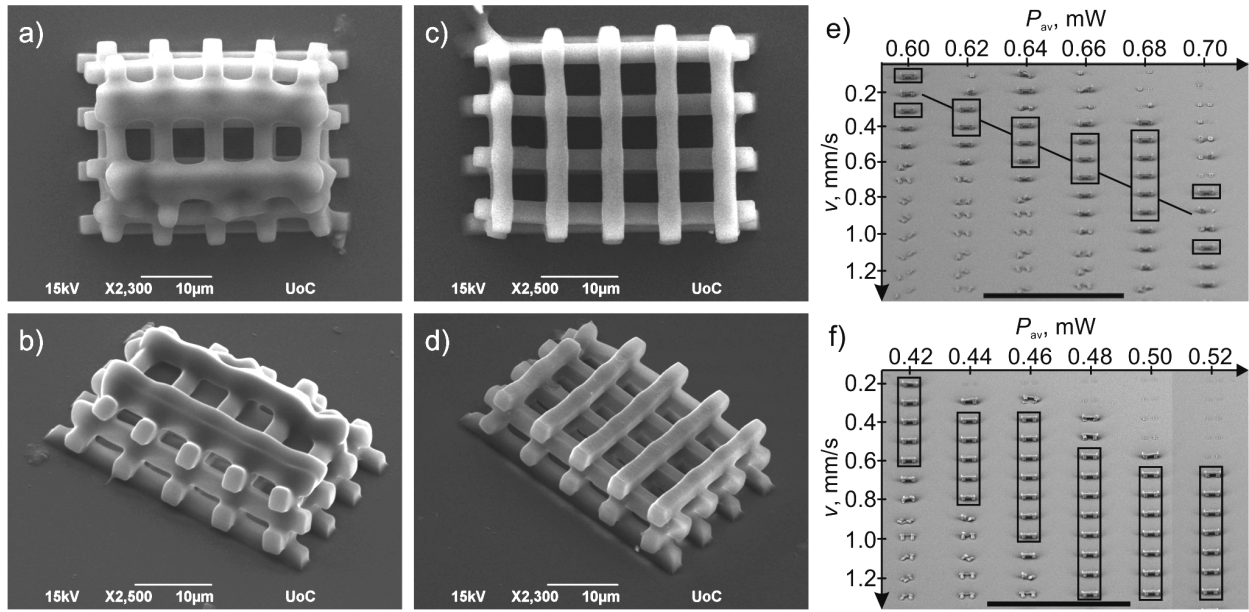


Figure 6.1: 3D structures fabricated out of PDMS+1% ISO using Ti:Sapphire laser system by employing a)-b) increasing power algorithm and c)-d) double scanning algorithm. 3D structures' array fabricated using Yb:KGW laser system out of e) pure PDMS and f) PDMS+0.5% ISO (scale bar – 200 μm).

The samples were exposed to $P_{av} = 53 \text{ mW}$ ($I_p = 4.35 \text{ TW}/\text{cm}^2$) laser radiation hoping to observe polymerization by scanning the beam inside pre-polymer ($v < 10 \mu\text{m}/\text{s}$).

2. *The PIs' solubility tests in PDMS.* PIs, which supported polymerization in PDMS (ISO, TPO, TPO-L, IRG, BISM and THIO) were mixed in larger quantities. Thus, a 1% doping of PDMS using ISO, TPO and TPO-L photo-initiators was achieved without visually observing changes to the mixture's homogeneity.

3. *Fabrication of 2D gratings.* The mixtures with maximum doping were used for 2D grating fabrication. The structures fabricated out of PDMS doped with THIO, IRG and ISO photo-initiators survived the development process. ISO PI was chosen for further experiments since the used velocities at the same fabrication parameters were achieved higher than for other PIs (thus, the throughput was also higher).

4. *Fabrication of 3D structures.* PDMS doped with 1% ISO was used for the fabrication of woodpile type structures. Since the PDMS is liquid, the structuring was performed starting from the substrate so the distant layers were fabricated by a laser beam defocused by passing through the already polymerized areas. Two methods were used to solve this: 1) higher laser power was used to fabricate the more distant layers (see Figure 6.1 a)-b), fabrication parameters: $dxy = 0.2 \mu\text{m}$, $dz = 0.5 \mu\text{m}$, $v = 150 \mu\text{m}/\text{s}$, the used average laser power for the first-second, third-fourth and fifth layers respectively were $P_{av} = 62\text{--}64\text{--}67 \text{ mW}$ ($I_p = 5.09\text{--}5.25\text{--}5.50 \text{ TW}/\text{cm}^2$), the achieved 3D structuring throughput – $20 \mu\text{m}^3/\text{s}$) or 2) the distant layers scanned twice (see Figure 6.1 c)-d), fabrication parameters: $dxy = 0.2 \mu\text{m}$, $dz = 0.5 \mu\text{m}$, $v = 150 \mu\text{m}/\text{s}$, all layers fabricated using $P_{av} = 64 \text{ mW}$ ($I_p = 5.25 \text{ TW}/\text{cm}^2$) and for the last two additional scanning using 55 mW ($I_p = 4.51 \text{ TW}/\text{cm}^2$) was performed, 3D structuring throughput – $15 \mu\text{m}^3/\text{s}$). Better results (lower shrinkage of the distant layers) were acquired using the latter method.

6.2 Structuring Using Yb:KGW Laser System

The experiments were performed using three different types of samples – pure PDMS, doped with 0.5% ISO, which demonstrated the best results using Ti:Sapphire system, and doped with 0.2% THIO, which has a two-photon absorption band for 515 nm. The arrays of the same structure – gate, consisting of two vertical rods and a horizontal one on the top, – were fabricated with $dxy = 0.3 \mu\text{m}$ and $dz = 0.4 \mu\text{m}$. Arrays fabricated using pure (e) and doped with 0.5% PDMS (f) are shown in Figure 6.1. The rectangles mark structures of good quality (not caved in or exploded). It is clear that the fabrication window of doped PDMS is much broader.

It was noticed that the manner in which the laser beam's position inside the sample is changed has a significant influence on the quality of the structures and on the 3D fabrication throughput. When fabricating using only linear motion stages, grainy, uneven surface is observed if high fabrication velocities ($>1 \text{ mm/s}$) are used due to the inertia of liquid PDMS. In order to fabricate structures well corresponding to the CAD model, IFV regime must be used. Also, slow beam scanning velocity ($\approx 100 \mu\text{m/s}$) should be used in order to achieve a high degree of cross-linking and acquire a structure having well-defined and not rounded corners. If linear stages are used for fabrication structures of good quality are acquired with sample translation velocities up to 1.0 mm/s ($P_{av} = 0.68 \text{ mW}$, $I_p = 1.63 \text{ TW/cm}^2$, 3D fabrication throughput – $120 \mu\text{m}^3/\text{s}$) for PDMS doped with 0.2% THIO; 1.5 mm/s ($P_{av} = 0.5 \text{ mW}$, $I_p = 1.20 \text{ TW/cm}^2$, 3D fabrication throughput – $180 \mu\text{m}^3/\text{s}$) for PDMS doped with 0.5% ISO; 1.0 mm/s ($P_{av} = 0.7 \text{ mW}$, $I_p = 1.68 \text{ TW/cm}^2$, 3D fabrication throughput $120 \mu\text{m}^3/\text{s}$) for pure PDMS. If the IFV regime is used, the throughputs increase to $180 \mu\text{m}^3/\text{s}$ for pure PDMS and doped with 0.2% THIO ($v = 1.5 \text{ mm/s}$) and $720 \mu\text{m}^3/\text{s}$ ($v = 6 \text{ mm/s}$) for PDMS doped with 0.5% ISO.

6.3 Polymerization Initiation Mechanisms in PDMS

Modeling of the free electron generation dynamics (Figure 6.2, calculated according to the equations in Section 1.2)⁴ showed that in the case of Ti:Sapphire laser system the main source for the free electron generation in both doped and pure PDMS is

Table 6.2: The rates of multi-photon and avalanche ionization in PDMS.

λ , nm	PI	I_p , TW/cm ²	n_{ph}	w_{mpi} , $\times 10^{10} \text{ s}^{-1}$	w_{imp} , $\times 10^{10} \text{ s}^{-1}$
515	–	1.6	3	0.004	299
	ISO, THIO	1.2	2	2.65	374
800	–	5.2	4	0.019	2263
	ISO, THIO		3	5.74	3772

⁴Note that the presented graphs are qualitative and only demonstrate how specific ionization rate values influence the free electron generation for the pulses of different duration; they are not suitable for quantitative assessment.

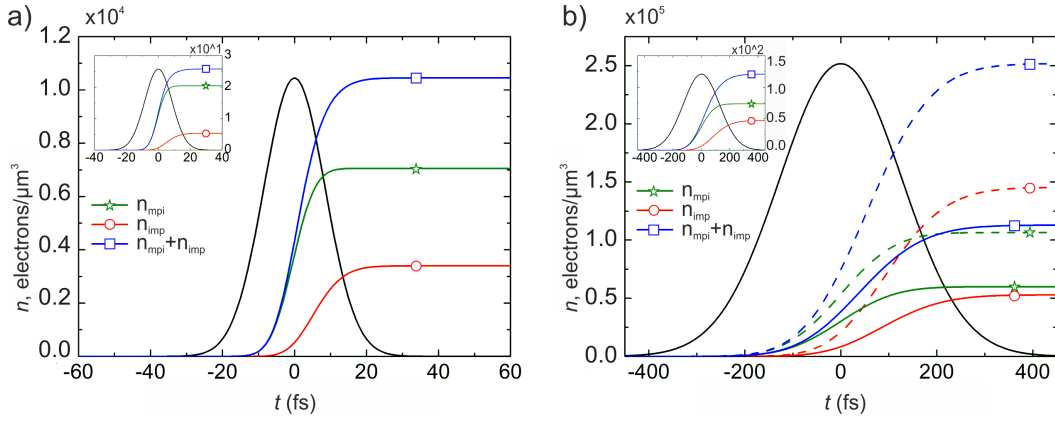


Figure 6.2: The calculated free electron generation dynamics due to multi-photon and avalanche ionization (n_{mpi} and n_{imp}) in PDMS. a) For Ti:Sapphire laser system, when $I_p = 5.2 \text{ TW/cm}^2$; pure PDMS in the inset. b) For Yb:KGW laser system when $I_p = 1.2 \text{ TW/cm}^2$ (polymerization, solid lines) and $I_p = 1.6 \text{ TW/cm}^2$ (breakdown, dashed lines); pure PDMS in the inset, $I_p = 1.6 \text{ TW/cm}^2$ (polymerization).

multi-photon absorption (Figure 6.2 a), although the rate of avalanche ionization is much higher (see Table 6.2, $w_{imp} \gg w_{mpi}$). For the pure PDMS the 4-photon absorption is not efficient and, although the free electron generation rate for the avalanche ionization is five orders higher than that for the multi-photon ionization, due to the short pulse the avalanche does not switch on, and there are not enough radicals to initiate the polymerization. However, doping with PIs creates a more efficient and controllable source of free electrons in the form of 3-photon absorption which is sufficient for the polymerization to commence. On the other hand, a slightly different situation is in the case of Yb:KGW laser system. At the typical fabrication intensities ($\approx 1.2 \text{ TW/cm}^2$, Figure 6.2 b), solid lines) the dominant free electron generation mechanism is multi-photon ionization, which is quite efficient in both doped and pure PDMS. However, at the breakdown intensities of the doped PDMS ($\approx 1.6 \text{ TW/cm}^2$, Figure 6.2 b), dashed lines) avalanche ionization becomes dominant and results in micro-explosions during fabrication.

In both cases doping of the PDMS with PIs increases the effectiveness of multi-photon absorption making polymerization more efficient using the Yb:KGW and possible with Ti:Sapphire laser system.

6.4 Conclusions

3D structuring of PDMS doped with ISO photo-initiator can be performed using Ti:Sapphire laser system with a throughput of $20 \mu\text{m}^3/\text{s}$. Using Yb:KGW laser system the highest throughput was reached for PDMS doped with the same PI and was $720 \mu\text{m}^3/\text{s}$ when IFV regime was used; it is 60 times larger as compared to the other groups' results. Also, for the first time laser structuring of pure PDMS without any additives was reported. The performed theoretical calculations show that multi-photon absorption is the dominant mechanism in breaking the chemical bonds in all cases of successful laser fabrication.

Conclusions

1. The width of the suspended lines fabricated out of SZ2080, OrmoComp and PETA pre-polymers using linearly polarized light is the biggest when the angle between the polarization vector and the sample translation direction is $\alpha = 90^\circ$ and smallest when $\alpha = 0^\circ$. This is consistent with the results of theoretical simulation of the focusing using high numerical aperture ($NA > 1.35$) objective, performed by employing vectorial Debye theory, according to which the intensity distribution is elongated along the polarization direction. The experimental investigation of the aforementioned pre-polymers showed that the difference between the thinnest and the widest lines can reach up to 20%.
2. The lines fabricated out of SZ2080, OrmoComp and PETA using circularly polarized light have smaller lateral dimensions than the lines formed using linearly polarized light. The investigation of the axial resolution in SZ2080 pre-polymer showed that is also higher which might be attributed to smaller multi-photon absorption cross-section of the materials for the circular polarization.
3. It was experimentally shown that the direction of the linearly polarized light's electric field vector does not influence the axial resolution of the lines. Thus control of the polarization direction makes it possible to dynamically tune the aspect ratio of the fabricated structures.
4. Structures fabricated by DLW in pre-polymers undergo reversible deformations (swelling and shrinking) when placed in liquid environment. These tendencies are valid at least as long as the lateral dimensions of the polymeric lines do not exceed $1.5 \mu\text{m}$. Based on this property sensors and micro-manipulators were demonstrated which stayed sensitive to the environment after several liquid exchange cycles.
5. The DLW in pre-polymers method can be used to fabricate composite structures out of up to four different pre-polymers without any observable influence to the final structure's quality. An addition of the second material is possible in a freely chosen position in all three dimensions. Combination of the composite material fabrication with reversible deformations of polymeric elements enables to take advantage of the different properties of the two materials in formation of bi-polymeric sensors.
6. Pure SZ2080 and doped with 1% IRG photo-initiator is suitable for the fabrication of high number micro-structured scaffolds for statistical cell growth experiments. Up to $2.1 \times 2.1 \times 0.21 \text{ mm}^3$ volume scaffolds of hexagonal and rectangular type can be fabricated with the throughput of $27500 \mu\text{m}^3/\text{s}$ and $51300 \mu\text{m}^3/\text{s}$ respectively out of doped SZ2080. A throughput of $16400 \mu\text{m}^3/\text{s}$ can be achieved for the rectangular type scaffold out of pure SZ2080. *In vivo* experiments show that the hexagonal type scaffolds are suitable for the regeneration of articular cartilage and demonstrate better results than commonly used collagen membranes.

7. 3D structuring of the biocompatible elastomer PDMS doped with ISO photo-initiator is possible using Ti:Sapphire laser system with throughput of $20 \mu\text{m}^3/\text{s}$ and using Yb:KGW laser system – $720 \mu\text{m}^3/\text{s}$. 3D structuring of pure PDMS using Yb:KGW laser system can be achieved with throughput of $180 \mu\text{m}^3/\text{s}$. Better results achieved using photo-sensitized PDMS can be explained by the fact that doping with PI creates a controllable generation of free electrons due to multi-photon absorption as was shown by theoretical calculations.

Bibliography

1. S. Maruo, O. Nakamura, S. Kawata, Three-dimensional microfabrication with two-photon-absorbed photopolymerization, *Opt. Lett.* **22**(2), 132 (1997).
2. W. Haske, V. W. Chen, J. M. Hales, W. Dong, S. Barlow, S. R. Marder, J. W. Perry, 65 nm feature sizes using visible wavelength 3-D multiphoton lithography, *Opt. Express* **15**(6), 3426 (2007).
3. P. Danilevicius, S. Rekstyte, E. Balciunas, A. Kraniauskas, R. Jarasiene, R. Sirmenis, D. Baltriukiene, V. Bukelskiene, R. Gadonas, M. Malinauskas, Microstructured polymer scaffolds fabricated by direct laser writing for tissue engineering, *J. Biomed. Opt.* **17**(8), 0814051–0814057 (2012).
4. www.nanoscribe.de (tikrinta 2016-05-24).
5. C. N. LaFratta, J. T. Fourkas, T. Baldacchini, R. A. Farrer, Multiphoton fabrication, *Angew. Chem. Int. Ed.* **46**(33), 6238–6258 (2007).
6. S. Maruo, J. Fourkas, Recent progress in multiphoton microfabrication, *Laser Photon. Rev.* **2**(1-2), 100–111 (2008).
7. T. Weiß, G. Hildebrand, R. Schade, K. Liefeth, Two-photon polymerization for microfabrication of three-dimensional scaffolds for tissue engineering application, *Eng. Life Sci.* **9**(5), 384–390 (2009).
8. G. von Freymann, A. Ledermann, M. Thiel, I. Staude, S. Essig, K. Busch, M. Wegener, Three-dimensional nanostructures for photonics, *Adv. Funct. Mater.* **20**(7), 1038–1052 (2010).
9. S. M. Eaton, C. De Marco, R. Martinez-Vazquez, R. Ramponi, S. Turri, G. Cerullo, R. Osellame, Femtosecond laser microstructuring for polymeric lab-on-chips, *J. Biophotonics* **5**(8-9), 687–702 (2012).
10. D. S. Correa, M. R. Cardoso, V. Tribuzi, L. Misoguti, C. R. Mendonça, Femtosecond laser in polymeric materials: Microfabrication of doped structures and micromachining, *IEEE J. Sel. Top. Quantum Electron.* **18**(1), 176–186 (2012).
11. A. Selimis, V. Mironov, M. Farsari, Direct laser writing: Principles and materials for scaffold 3D printing, *Microelectron. Eng.* **132**, 83–89 (2015).
12. X. Zhou, Y. Hou, J. Lin, A review on the processing accuracy of two-photon polymerization, *AIP Advances* **5**(3), 030701 (2015).
13. I. Roy, M. N. Gupta, Smart polymeric materials, *Chem. Biol.* **10**(12), 1161–1171 (2003).
14. Z. X. Khoo, J. E. M. Teoh, Y. Liu, C. K. Chua, S. Yang, J. An, K. F. Leong, W. Y. Yeong, 3D printing of smart materials: A review on recent progresses in 4D printing, *Virtual. Phys. Prototyp.* **10**(3), 103–122 (2015).
15. U. Okoroanyanwu, in *Chemistry and Lithography* (SPIE, 2010).
16. M. Thiel, J. Fischer, G. von Freymann, M. Wegener, Direct laser writing of three-dimensional submicron structures using a continuous-wave laser at 532 nm, *Appl. Phys. Lett.* **97**(22), 221102 (2010).

-
17. I. Wang, M. Bouriau, P. L. Baldeck, C. Martineau, C. Andraud, Three-dimensional microfabrication by two-photon-initiated polymerization with a low-cost microlaser, *Opt. Lett.* **27**(15), 1348 (2002).
 18. H.-B. Sun, S. Kawata, Two-photon laser precision microfabrication and its applications to micro-nano devices and systems, *J. Lightwave Technol.* **21**(3), 624–633 (2003).
 19. M. Malinauskas, A. Žukauskas, G. Bičkauskaitė, R. Gadonas, S. Juodkazis, Mechanisms of three-dimensional structuring of photo-polymers by tightly focussed femtosecond laser pulses, *Opt. Express* **18**(10), 10209–10221 (2010).
 20. M. Malinauskas, P. Danilevičius, S. Juodkazis, Three-dimensional micro-/nano-structuring via direct write polymerization with picosecond laser pulses, *Opt. Express* **19**(6), 5602 (2011).
 21. T. Baldacchini, S. Snider, R. Zadoyan, Two-photon polymerization with variable repetition rate bursts of femtosecond laser pulses, *Opt. Express* **20**(28), 29890 (2012).
 22. J. B. Mueller, J. Fischer, Y. J. Mange, T. Nann, M. Wegener, In-situ local temperature measurement during three-dimensional direct laser writing, *Appl. Phys. Lett.* **103**(12), 123107 (2013).
 23. J. Fischer, J. B. Mueller, J. Kaschke, T. J. A. Wolf, A.-N. Unterreiner, M. Wegener, Three-dimensional multi-photon direct laser writing with variable repetition rate, *Opt. Express* **21**(22), 26244 (2013).
 24. M. Malinauskas, M. Farsari, A. Piskarskas, S. Juodkazis, Ultrafast laser nanostructuring of photopolymers: A decade of advances, *Phys. Rep.* **533**(1), 1–31 (2013).
 25. H. Misawa, S. Juodkazis, *3D laser microfabrication: principles and applications* (John Wiley & Sons, 2006).
 26. I. Ftilis, M. Fakis, I. Polyzos, V. Giannetas, P. Persephonis, Two-photon polymerization of a diacrylate using fluorene photoinitiators–sensitizers, *J. Photoch. Photobio. A* **215**(1), 25–30 (2010).
 27. A. Ovsianikov, J. Viertl, B. Chichkov, M. Oubaha, B. MacCraith, I. Sakellari, A. Giakoumaki, D. Gray, M. Vamvakaki, M. Farsari, C. Fotakis, Ultra-low shrinkage hybrid photosensitive material for two-photon polymerization microfabrication, *ACS Nano* **2**(11), 2257–2262 (2008).
 28. T. Atsumi, J. Murata, I. Kamiyanagi, S. Fujisawa, T. Ueha, Cytotoxicity of photosensitizers camphorquinone and 9-fluorenone with visible light irradiation on a human submandibular-duct cell line in vitro, *Arch. Oral Biol.* **43**(1), 73–81 (1998).
 29. M. Sangermano, L. Vescovo, N. Pepino, A. Chiolerio, P. Allia, P. Tiberto, M. Coisson, L. Suber, G. Marchegiani, Photoinitiator-free UV-cured acrylic coatings containing magnetite nanoparticles, *Macromol. Chem. Phys.* **211**(23), 2530–2535 (2010).
 30. H. Selvaraj, B. Tan, K. Venkatakrisnan, Maskless direct micro-structuring of PDMS by femtosecond laser localized rapid curing, *J. Micromech. Microeng.* **21**(7), 075018 (2011).

-
31. N. B. Cramer, J. P. Scott, C. N. Bowman, Photopolymerizations of thiol-ene polymers without photoinitiators, *Macromolecules* **35**(14), 5361–5365 (2002).
 32. N. B. Cramer, S. K. Reddy, M. Cole, C. Hoyle, C. N. Bowman, Initiation and kinetics of thiol-ene photopolymerizations without photoinitiators, *J. Polym. Sci., Part A: Polym. Chem.* **42**(22), 5817–5826 (2004).
 33. S. Aliwi, C. Bamford, Photoactive polymers containing vanadium: 1. Preparation, characterization and photoreactions, *Polymer* **18**(4), 375–380 (1977).
 34. J. Xue, Y. Zhao, J. Wu, F. Wu, Novel benzylidene cyclopentanone dyes for two-photon photopolymerization, *J. Photochem. Photobiol. A* **195**(2), 261–266 (2008).
 35. G. Witzgall, R. Vrijen, E. Yablonovitch, V. Doan, B. J. Schwartz, Single-shot two-photon exposure of commercial photoresist for the production of three-dimensional structures, *Opt. Lett.* **23**(22), 1745 (1998).
 36. S. Maruo, A. Takaura, Y. Saito, Optically driven micropump with a twin spiral microrotor, *Opt. Express* **17**(21), 18525 (2009).
 37. K. Kuetemeyer, G. Kensah, M. Heidrich, H. Meyer, U. Martin, I. Gruh, A. Heisterkamp, Two-photon induced collagen cross-linking in bioartificial cardiac tissue, *Opt. Express* **19**(17), 15996 (2011).
 38. O. Kufelt, A. El-Tamer, C. Sehring, M. Meißner, S. Schlie-Wolter, B. N. Chichkov, Water-soluble photopolymerizable chitosan hydrogels for biofabrication via two-photon polymerization, *Acta Biomater.* **18**, 186–195 (2015).
 39. O. Kufelt, A. El-Tamer, C. Sehring, S. Schlie-Wolter, B. N. Chichkov, Hyaluronic acid based materials for scaffolding via two-photon polymerization, *Biomacromolecules* **15**(2), 650–659 (2014).
 40. S. Basu, P. J. Campagnola, Properties of crosslinked protein matrices for tissue engineering applications synthesized by multiphoton excitation, *J. Biomed. Mater. Res.* **71A**(2), 359–368 (2004).
 41. J. D. Pitts, P. J. Campagnola, G. A. Epling, S. L. Goodman, Submicron multiphoton free-form fabrication of proteins and polymers: studies of reaction efficiencies and applications in sustained release, *Macromolecules* **33**(5), 1514–1523 (2000).
 42. E. Kämpylä, T. Sedláčik, D. B. Aydogan, J. Viitanen, F. Rypáček, M. Kellomäki, Direct laser writing of synthetic poly(amino acid) hydrogels and poly(ethylene glycol) diacrylates by two-photon polymerization, *Mater. Sci. Eng. C* **43**, 280–289 (2014).
 43. W. Zhang, S. Chen, Femtosecond laser nanofabrication of hydrogel biomaterial, *MRS Bull.* **36**(12), 1028–1033 (2011).
 44. R. Houbertz, S. Steenhusen, T. Stichel, G. Sextl, *Two-photon polymerization of inorganic-organic hybrid polymers as scalable technology using ultra-short laser pulses*, volume 7 (InTech, 2010).
 45. F. Klein, B. Richter, T. Striebel, C. M. Franz, G. von Freymann, M. Wegener, M. Bastmeyer, Two-component polymer scaffolds for controlled three-dimensional cell culture, *Adv. Mat.* **23**(11), 1341–1345 (2011).
 46. A. Ovsianikov, S. Schlie, A. Ngezahayo, A. Haverich, B. N. Chichkov, Two-photon polymerization technique for microfabrication of CAD-designed 3D scaffold

-
- folds from commercially available photosensitive materials, *J. Tissue Eng. Regen. Med.* **1**(6), 443–449 (2007).
47. M. Deubel, G. von Freymann, M. Wegener, S. Pereira, K. Busch, C. M. Soukoulis, Direct laser writing of three-dimensional photonic-crystal templates for telecommunications, *Nat. Mater.* **3**(7), 444–447 (2004).
 48. www.sartomer.com (tikrinta 2016-05-12).
 49. A. Lasagni, D. Yuan, P. Shao, S. Das, Fabrication of periodic microstructures in pentaerythritol triacrylate through femtosecond laser interference two-photon polymerization, *Adv. Eng. Mater.* **11**(7), 595–599 (2009).
 50. A. J. G. Otuka, J. M. P. Almeida, V. Tribuzi, M. R. Cardoso, A. C. Hernandez, D. S. Correa, C. R. Mendonça, Femtosecond lasers for processing glassy and polymeric materials, *Mat. Res.* **17**(2), 352–358 (2014).
 51. P. Tayalia, C. R. Mendonça, T. Baldacchini, D. J. Mooney, E. Mazur, 3D cell-migration studies using two-photon engineered polymer scaffolds, *Adv. Mater.* **20**(23), 4494–4498 (2008).
 52. F. Schneider, J. Draheim, R. Kamberger, U. Wallrabe, Process and material properties of polydimethylsiloxane (PDMS) for optical MEMS, *Sensor Actuat. A-Phys.* **151**(2), 95–99 (2009).
 53. W.-C. Tian, E. Finehout, *Microfluidics for biological applications*, volume 16 (Springer Science & Business Media, 2009).
 54. D. Cai, A. Neyer, R. Kuckuk, H. Heise, Optical absorption in transparent PDMS materials applied for multimode waveguides fabrication, *Opt. Mater.* **30**(7), 1157–1161 (2008).
 55. T. C. Merkel, V. I. Bondar, K. Nagai, B. D. Freeman, I. Pinnau, Gas sorption, diffusion, and permeation in poly(dimethylsiloxane), *J. Polym. Sci. Polym. Phys.* **38**(3), 415–434 (2000).
 56. D. Armani, C. Liu, N. Aluru, Re-configurable fluid circuits by PDMS elastomer micromachining, in *Proc. of the IEEE Micro Electro Mechanical Systems* (IEEE, 1999), 222–227.
 57. M.-C. Bélanger, Y. Marois, Hemocompatibility, biocompatibility, inflammatory and in vivo studies of primary reference materials low-density polyethylene and polydimethylsiloxane: A review, *J. Biomed. Mater. Res.* **58**(5), 467–477 (2001).
 58. C. T. Pan, Y. C. Chen, P.-H. Lin, C. C. Hsieh, F. T. Hsu, P.-H. Lin, C. M. Chang, J. H. Hsu, J. C. Huang, Lens of controllable optical field with thin film metallic glasses for UV-LEDs, *Opt. Express* **22**(12), 14411 (2014).
 59. J. C. McDonald, D. C. Duffy, J. R. Anderson, D. T. Chiu, H. Wu, O. J. A. Schueller, G. M. Whitesides, Fabrication of microfluidic systems in poly(dimethylsiloxane), *Electrophoresis* **21**(1), 27–40 (2000).
 60. J. C. McDonald, G. M. Whitesides, Poly(dimethylsiloxane) as a material for fabricating microfluidic devices, *Acc. Chem. Res.* **35**(7), 491–499 (2002).
 61. <http://www.femtika.lt/software/> (tikrinta 2016-05-12).
 62. J. Bonse, J. Krüger, S. Höhm, A. Rosenfeld, Femtosecond laser-induced periodic surface structures, *J. Laser Appl.* **24**(4), 042006 (2012).
 63. Y. Tang, J. Yang, B. Zhao, M. Wang, X. Zhu, Control of periodic ripples growth on metals by femtosecond laser ellipticity, *Opt. Express* **20**(23), 25826 (2012).

-
64. A. Borowiec, H. K. Haugen, Subwavelength ripple formation on the surfaces of compound semiconductors irradiated with femtosecond laser pulses, *Appl. Phys. Lett.* **82**(25), 4462 (2003).
 65. R. Buividas, L. Rosa, R. Šliupas, T. Kudrius, G. Šlekys, V. Datsyuk, S. Juodkazis, Mechanism of fine ripple formation on surfaces of (semi)transparent materials via a half-wavelength cavity feedback, *Nanotechnology* **22**(5), 055304 (2010).
 66. J. Reif, F. Costache, M. Henyk, S. V. Pandelov, Ripples revisited: Non-classical morphology at the bottom of femtosecond laser ablation craters in transparent dielectrics, *Appl. Surf. Sci.* **197–198**, 891–895 (2002).
 67. S. Baudach, J. Bonse, W. Kautek, Ablation experiments on polyimide with femtosecond laser pulses, *Appl. Phys. A Mater. Sci. Process.* **69**(7), S395–S398 (1999).
 68. S. Yada, M. Terakawa, Femtosecond laser induced periodic surface structure on poly-l-lactic acid, *Opt. Express* **23**(5), 5694 (2015).
 69. K. Venkatakrisnan, B. Tan, P. Stanley, N. R. Sivakumar, The effect of polarization on ultrashort pulsed laser ablation of thin metal films, *J. Appl. Phys.* **92**(3), 1604 (2002).
 70. H.-B. Sun, M. Maeda, K. Takada, J. W. M. Chon, M. Gu, S. Kawata, Experimental investigation of single voxels for laser nanofabrication via two-photon photopolymerization, *Appl. Phys. Lett.* **83**(5), 819 (2003).
 71. P. Török, P. Varga, Electromagnetic diffraction of light focused through a stratified medium, *Appl. Opt.* **36**(11), 2305 (1997).
 72. M. J. Nasse, J. C. Woehl, Realistic modeling of the illumination point spread function in confocal scanning optical microscopy, *J. Opt. Soc. Am. A* **27**(2), 295 (2010).
 73. A. Ovsianikov, X. Shizhou, M. Farsari, M. Vamvakaki, C. Fotakis, B. Chichkov, Shrinkage of microstructures produced by two-photon polymerization of Zr-based hybrid photosensitive materials, *Opt. Express* **17**(4), 2143 (2009).
 74. X.-M. Takada, KDuan, Q.-D. Chen, S. Shoji, H. Xia, S. Kawata, H.-B. Sun, Size-dependent behaviors of femtosecond laser-prototyped polymer micronanowires, *Opt. Lett.* **34**(5), 566–568 (2009).
 75. Q. Sun, K. Ueno, H. Misawa, In situ investigation of the shrinkage of photopolymerized micro/nanostructures: the effect of the drying process, *Opt. Lett.* **37**(4), 710 (2012).
 76. S. Kuebler, A. Narayanan, D. Karas, K. Wilburn, Low-distortion surface functionalization of polymeric microstructures, *Macromol. Chem. Phys.* **215**(16), 1533–1542 (2014).
 77. C. Py, P. Reverdy, L. Doppler, J. Bico, B. Roman, C. N. Baroud, Capillary origami: Spontaneous wrapping of a droplet with an elastic sheet, *Phys. Rev. Lett.* **98**(15) (2007).
 78. S. Felton, M. Tolley, B. Shin, C. Onal, E. Demaine, D. Rus, R. Wood, Self-folding with shape memory composites, *Soft Matter*. **9**(32), 7688–7694 (2013).
 79. T. Campbell, S. Tibbits, B. Garrett, The programmable world, *Sci. Amer.* **311**, 60–65 (2014).

-
80. Z. Xiong, M.-L. Zheng, X.-Z. Dong, W.-Q. Chen, F. Jin, Z.-S. Zhao, X.-M. Duan, Asymmetric microstructure of hydrogel: two-photon microfabrication and stimuli-responsive behavior, *Soft Matter*. **7**(21), 10353 (2011).
 81. Y. Tian, Y.-L. Zhang, H. Xia, L. Guo, J.-F. Ku, Y. He, R. Zhang, B.-Z. Xu, Q.-D. Chen, H.-B. Sun, Solvent response of polymers for micromachine manipulation, *Phys. Chem. Chem. Phys.* **13**(11), 4835 (2011).
 82. Y. Da Sie, Y.-C. Li, N.-S. Chang, P. J. Campagnola, S.-J. Chen, Fabrication of three-dimensional multi-protein microstructures for cell migration and adhesion enhancement, *Biomed. Opt. Express* **6**(2), 480 (2015).
 83. J. R. Wolter, R. Meyer, Sessile macrophages forming clear endothelium-like membrane on inside of successful keratoprosthesis, *Trans. Am. Ophthalmol. Soc.* **82**, 187 (1984).
 84. R. Langer, J. Vacanti, Tissue engineering, *Science* **260**(5110), 920–926 (1993).
 85. B. P. Chan, K. W. Leong, Scaffolding in tissue engineering: general approaches and tissue-specific considerations, *Eur. Spine J.* **17**(S4), 467–479 (2008).
 86. J. Torgersen, A. Ovsianikov, V. Mironov, N. Pucher, X. Qin, Z. Li, K. Cicha, T. Machacek, R. Liska, V. Jantsch, et al., Photo-sensitive hydrogels for three-dimensional laser microfabrication in the presence of whole organisms, *J. Biomed. Opt.* **17**(10), 105008 (2012).
 87. T. Weiss, R. Schade, T. Laube, A. Berg, G. Hildebrand, R. Wyrwa, M. Schnabelrauch, K. Liefelth, Two-photon polymerization of biocompatible photopolymers for microstructured 3D biointerfaces, *Adv. Eng. Mater.* **13**(9), B264–B273 (2011).
 88. A. Matei, M. Zamfirescu, C. Radu, E. C. Buruiana, T. Buruiana, C. Mustaciosu, I. Petcu, M. Radu, M. Dinescu, Producing ORMOSIL scaffolds by femtosecond laser polymerization, *Appl. Phys. A* **108**(1), 91–97 (2012).
 89. V. Melissinaki, A. A. Gill, I. Ortega, M. Vamvakaki, A. Ranella, J. W. Haycock, C. Fotakis, M. Farsari, F. Claeysens, Direct laser writing of 3D scaffolds for neural tissue engineering applications, *Biofabrication* **3**(4), 045005 (2011).
 90. M. T. Raimondi, S. M. Eaton, M. Laganá, V. Aprile, M. M. Nava, G. Cerullo, R. Osellame, Three-dimensional structural niches engineered via two-photon laser polymerization promote stem cell homing, *Acta Biomater.* **9**(1), 4579–4584 (2013).
 91. R. N. Palchesko, L. Zhang, Y. Sun, A. W. Feinberg, Development of polydimethylsiloxane substrates with tunable elastic modulus to study cell mechanobiology in muscle and nerve, *PLoS ONE* **7**(12), e51499 (2012).
 92. C. T. McKee, J. A. Last, P. Russell, C. J. Murphy, Indentation versus tensile measurements of young's modulus for soft biological tissues, *Tissue Eng. Part B Rev.* **17**(3), 155–164 (2011).
 93. C. Coenjarts, C. Ober, Two-photon three-dimensional microfabrication of poly(dimethylsiloxane) elastomers, *Chem. Mater.* **16**(26), 5556–5558 (2004).
 94. T. Hasegawa, K. Oishi, S. Maruo, Three-dimensional microstructuring of PDMS by two-photon microstereolithography, *IEEE* **06**, 158–161 (2006).
 95. D.-X. Lu, Y.-L. Zhang, D.-D. Han, H. Wang, H. Xia, Q.-D. Chen, H. Ding, H.-B. Sun, Solvent-tunable PDMS microlens fabricated by femtosecond laser direct writing, *J. Mater. Chem. C* **3**(8), 1751–1756 (2015).

Santrauka

TIESIOGINIO LAZERINIO RAŠYMO FEMTOSEKUNDINIAIS ŠVIESOS IMPULSAIS SKAIDRIOSE TINKLINAMOSE MEDŽIAGOSE METODŲ VYSTYMAS IR TAIKYMAI

Tiesioginis lazerinis rašymas skaidriose tinklinamose medžiagose, pagrįstas netiesine šviesos bei medžiagos sąveika, yra vienas plačiausiai naudojamų polimerinių mikrodarinių formavimo būdų, užtikrinantis aukštą erdvinę raišką, pasižymintis plačiu apdirbamų medžiagų spektru, geometrijos parinkimo laisvumu bei mastelio derinimu plačiame intervale. Šios bei kitos savybės nulėmė, kad TLR metodu suformuoti dariniai rado pritaikymus pačiose įvairiausios sferose, tarp jų fotonikoje, mikrooptikoje, jutiklių gamyboje, medicinoje bei kitose.

Šiame disertaciniame darbe yra pristatomi eksperimentiniai tyrimai, pastūmėjantys TLR metodų vystymą dar arčiau realių praktinių taikymų. Atliekant tyrimus buvo kreipiamas ypatingas dėmesys skirtingų polimerų pirmtakų formavimo ypatumams. Nustatyta jų erdvinės formavimo raiškos priklausomybė nuo naudojamo lazerio pluošto poliarizacijos bei parodyta galimybė šį parametą panaudoti dinaminiam darinių aukščio ir pločio santykio derinimui. Iširtos polimerinių darinių, suformuotų TLR metodu, grįžtamosios deformacijos juos patalpinus įvairiose skystose terpėse. Šis efektas panaudotas aplinkai jautrių mikrojutiklių kūrimui. Be to, pristatoma galimybė gaminti polimerinius darinius iš kelių polimerų pirmtakų, prijungiamų skirtingų formavimų metu, sudaro galimybę praplėsti galutinių darinių funkcionalumą. Tai buvo pademonstruota šį metodą pritaikius bipolimerinio jutiklio formavimui.

Taip pat daug dėmesio skirta audinių inžinerijos taikymų sričiai. Parodytas TLR metodo tinkamumas polimerinių karkasų, skirtų audinių regeneracijos tyrimams *in vivo*, gamybai. Parodyta, kad optimizavus formavimo parametrus SZ2080 polimero pirmtake galima pasiekti trimačio formavimo našumus, pakankamus didelio kiekio milimetrų eilės mikrostruktūrizuotų konstrukčių gamybai. Su tokiais karkasais atlikti *in vitro* ir *in vivo* tyrimai parodė jų tinkamumą audinių inžinerijos taikymams (gauti geresni rezultatai regeneruojant kremzlės audinį nei su įprastai naudojamomis komercinėmis kolageninėmis membranomis), tad planuojami tolimesni darbai šioje srityje. Tam pradėti formuoti karkasai iš nefotojautrinto polimero pirmtako, skirti išsiaiškinti fotoiniciatoriaus įtaką ląstelių augimui; taip pat yra modifikuojama karkaso geometrija, porų formos įtakos nustatymui. Be to, atlikti lazerinio trimačių darinių formavimo iš medicininiams taikymams itin patrauklaus PDMS elastomero tyrimai leido pagerinti jo apdirbimo našumą 60 kartų bei priartino šio polimero pirmtako panaudojimą realioms taikymams.

Curriculum Vitae

Personal information

Name, Surname: Sima Rekštytė
Date of birth: 29 November 1987
Place of birth: Vilnius
E-mail: sima.rekstyte@gmail.com

Education

2012–2016 Vilnius University, Faculty of Physics, Department of Quantum Electronics. *PhD studies*
2010–2012 Vilnius University, Faculty of Physics. *Master degree*
2006–2010 Vilnius University, Faculty of Physics. *Bachelor degree*
1994–2006 Vilnius Žvėrynas Gymnasium (with honors)

Work experience

2013 01 – present Junior research fellow at Vilnius University
Laser Research Center
2011 07 – 2012 01 Engineer at Vilnius University
Laser Research Center
2009 04 – 2010 06 Laboratory assistant at Vilnius University
Department of Theoretical Physics

Internships

2014 08 – 2014 10 Shizuoka University (Japan)
2012 02 – 2012 07 IESL-FORTH Research Institute (Greece)

Additional information

Scholarships INFOBALT scholarship for young scientists, 2014
Awards Award for the oral presentation
Interdisciplinary Research in Physical and Technological Sciences conference
Vilnius, Lithuania, 2014
2nd place award for poster presentation
Lasers and Optical Nonlinearity conference
Vilnius, Lithuania, 2013
Young Scientist Award for poster presentation
Advanced Materials and Technologies conference
Palanga, Lithuania, 2011